J. Fluid Mech. (1996), *vol.* 313, *pp.* 1–38

Linear and nonlinear dynamics of a differentially heated slot under gravity modulation

By A. FAROOQ[1] AND G. M. HOMSY[2]

[1] Department of Mechanical Engineering, Stanford University, Stanford, CA 94305, USA

[2] Department of Chemical Engineering, Stanford University, Stanford, CA 94305, USA

(Received 10 November 1994 and in revised form 12 August 1995)

In this paper we consider the effect of sinusoidal gravity modulation of size ϵ on a differentially heated infinite slot in which a vertical temperature stratification is imposed on the walls. The slot problem is characterized by a Rayleigh number, Prandtl number, and the imposed uniform stratification on the walls. When ϵ is small, we show by regular perturbation expansion in ϵ that the modulation interacts with the natural mode of the system to produce resonances, confirming the results of Farooq & Homsy (1994). For $\epsilon \sim O(1)$ we show that the modulation can potentially destabilize the long-wave eigenmodes of the slot problem. This is achieved by projecting the governing equations onto the least-damped eigenmode, and investigating the resulting Mathieu equation via Floquet theory. No instability was found at large values of the Prandtl number and also low stratification, when there are no travelling modes present.

To understand the nonlinear saturation mechanisms of this growth, we consider a two-mode model of the slot problem with the primary mode being the least-damped travelling parallel-flow mode as before and a secondary mode of finite wavenumber. By projecting the governing equations onto these two modes we obtained the equations for temporal evolution of the two modes. For modulation amplitudes above critical, the growth of the primary mode is saturated resulting in a stable weak nonlinear synchronous oscillation of the primary mode. An unexpected and intriguing feature of the coupling is that the secondary mode exhibits very high-frequency bursts which appear once every cycle of the forcing frequency.

1. Introduction

This is a study of the effect of complex body forces on fluid motion. Such forces can arise in a number of ways, for example when a system with density gradients is subjected to vibrations. The resulting buoyancy forces, which are produced by the interaction of density gradients with the acceleration field, have a complex spatio–temporal structure depending on both the nature of density gradients and the spatial and frequency distribution of the vibration-induced acceleration field. Recently there has been a great deal of interest in the effects of such forces on fluid motion in connection with the effect of g-jitter, or residual spacecraft vibrations in space. There is a growing literature which tries to characterize the g-jitter environment, and recent reviews, e.g. Alexander (1990) and Nelson (1991), give a good summary of the earlier work on the subject. There have been a number of studies to investigate the effect of g-jitter on fluid motion, e.g. Amin (1988), Biringen & Peltier (1990), Biringen & Danabasoglu (1991), Alexander *et al.* (1991) and Farooq & Homsy (1994), who also provide references to much of the earlier work on the subject.

Since the aim of this study is to elucidate the physical mechanisms by which such

complex body forces operate, we analyse a simple model problem (to be described) and assume that the gravitational field has a simple form of the type

$$\boldsymbol{g}(\boldsymbol{x}, t) = g_0(1 + \epsilon \cos \Omega^* t)\,\boldsymbol{k}, \tag{1}$$

where $\boldsymbol{g}(\boldsymbol{x}, t)$ denotes the time-dependent gravitational field, g_0 is the mean gravitational field, Ω^* is the frequency of the single-harmonic component of oscillation, and $\boldsymbol{k}$ is the unit vector pointing vertically downward. Thus the gravitational field is seen to consist of a mean field and a single oscillatory term that corresponds to vertical oscillation of the system with scale ϵ and frequency Ω^*.

In an earlier study, Farooq & Homsy (1994) investigated the response of a differentially heated cavity to a time-dependent gravitation field of the type given by (1). However, the results were limited to the case where the aspect ratio of the cavity, A (defined as the ratio of the characteristic vertical dimension to the lateral dimension), was fixed at unity and the modulation scale, ϵ, was assumed to be small. Then by considering perturbation expansions in ϵ they were able to obtain a hierarchy of equations which were investigated in the parameter space consisting of the Rayleigh number, Ra, the Prandtl number, Pr, and the dimensionless forcing frequency, Ω, defined as

$$Ra = \frac{\alpha g_0 \Delta T D^3}{\nu\kappa}, \quad Pr = \frac{\nu}{\kappa}, \quad \Omega = \frac{\Omega^*}{g_0 \alpha \Delta T D/\nu};$$

ν and κ in the above expressions are the kinematic viscosity and the thermal diffusivity respectively, α is the coefficient of volumetric expansion, D and ΔT are the characteristic length and temperature scales.

They report that the response of the cavity, which consists of an $O(\epsilon)$ harmonic time-dependent part and an $O(\epsilon^2)$ steady-streaming part, shows a strong dependence on the frequency of the modulation. Strong resonances are reported at $O(\epsilon)$ when the forcing frequency matches the frequency of the natural eigenmodes of the system. However the $O(\epsilon^2)$ streaming response has been reported to show only very weak interaction with the natural modes. The response of both the components decays asymptotically as the forcing frequency becomes large. In this study we relax these two assumptions of small ϵ and aspect ratio fixed at unity by investigating $\epsilon \sim 1$ and including the effect of aspect ratio, A, as an additional parameter through a model slot problem.

It is interesting to consider the effect of the aspect ratio because as is well known from a number of studies treating the case of convection driven by a constant gravitational field, e.g. the classical work of Batchelor (1954), that the aspect ratio is an important determinant of the overall response of the system to the applied temperature gradient. Batchelor (1954) showed the existence of three regimes of flow depending on the parameters Ra, A: (i) the conduction regime, when Ra is low, A arbitrary; (ii) the boundary-layer regime, obtained in the limit $Ra \to \infty$, $A \sim O(1)$; and (iii) a transition regime which lies in between the two. Later Gill (1966) used boundary-layer theory to further investigate regime (ii) and showed that in this limit, the cavity is divided into two domains: boundary layers forming close to the lateral walls and a central core which shows vertical stratification of temperature. He showed that the boundary-layer thickness scaled as $(Ra/A)^{-1/4}$, and the core stratification varied inversely with the aspect ratio.

The stability of the steady two-dimensional laminar flow in a thermally driven cavity has an even stronger dependence on the aspect ratio. Paolucci & Chenoweth (1989) have done full two-dimensional numerical simulations for the transient heating problem and shown that A is a crucial parameter in determining the stability of the cavity and the particular modes that first become unstable. They report the existence

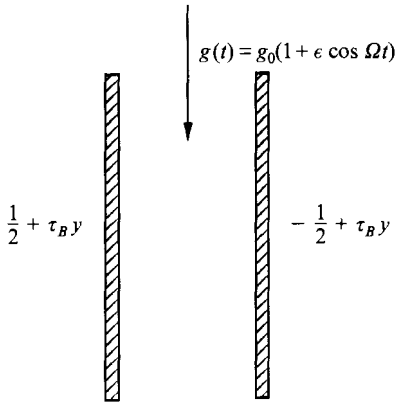

FIGURE 1. The geometry of the slot problem.

A	Ra_c	Critical mode
1	2×10^8	IW
2	3×10^7	IW
3	7×10^6	BL
4	2×10^6	BL
10	3×10^5	BL

TABLE 1. Data taken from Paolucci & Chenoweth (1989) that shows the competition between the IW and BL modes as the aspect ratio is varied, for $Pr = 0.71$.

of two kinds of travelling modes: travelling waves associated with the instability of the wall boundary layers, and internal gravity wave modes that represent sloshing motion of the stably stratified central core of the cavity. There is competition between these modes as the aspect ratio is varied. Table 1, which has data for $Pr = 0.71$, shows that the critical Rayleigh number, Ra_c, is strongly dependent on the aspect ratio of the cavity. Also the internal wave (IW) and boundary layer (BL) modes compete as the aspect ratio is varied, with the BL mode dominating at higher aspect ratios.

With regard to the gravity-modulated problem, the study of Farooq & Homsy (1994) while limited to $A = 1$ and small ϵ showed the possibility of resonances of the modulation with the characteristic internal wave modes of the system. Numerical constraints limited them to $Ra < 10^7$, and for this range of Ra they found strong interaction with internal wave modes present in the system. However, we know (from other works, see table 1 for example) that by suitably changing the aspect ratio, the boundary-layer mode can be made dominant. It is also conceivable that the two modes could be made to come in simultaneously, leading to the possibility of degenerate modes. Thus varying the parameter A leads to the prospect of interesting new possibilities which this study aims to understand.

In view of the numerical difficulties associated with the boundary-layer behaviour found in heated cavities, we consider a well-known model problem for tall cavities: an infinite differentially heated slot as shown in figure 1 with a constant vertical temperature stratification imposed on the walls. This slot problem, first proposed by Elder (1965) has since been extensively investigated to understand the stability behaviour of tall cavities when the gravity is held constant. The slot problem offers considerable advantage because the base flow is parallel, thus greatly simplifying the equations.

In this study, we wish to investigate the behaviour of this model slot problem in the presence of gravity modulation. We will proceed as follows. In §2 we will recount many of the well-known results for the slot problem for the constant-gravity case, with special emphasis on relating the results to well-known results for tall cavities. This section will provided much of the apparatus that will be used for the gravity-modulated problem.

We include the effect of modulation in three stages. In §3 we consider the effect of gravity modulation when ϵ is small allowing perturbation expansion of the variables, following Farooq & Homsy (1994). In §§4 and 5 we examine the effect of gravity modulation with $\epsilon \sim O(1)$, by considering the time-dependent evolution of the velocity and temperature fields using low-dimensional dynamical systems based on modal expansions. In §4 we consider a one-mode model and in §5 a two-mode model of the slot problem. Finally in §6 we offer a summary and some conclusions. The appropriate literature will be reviewed in each of the sections.

2. Slot problem: formulation and stability in the absence of gravity modulation

The slot problem consists of an infinite vertical slot, with a constant vertical temperature stratification, S, imposed on the boundaries, in addition to the constant lateral temperature drop, ΔT, across the walls (see figure 1). We will first develop the equations for the unmodulated problem, i.e. when $\epsilon = 0$. We use D, the slot width, as the characteristic lengthscale, $\nu/(g_0 \alpha \Delta T D)$ as the characteristic timescale, and ΔT is the temperature differential applied between the walls: ΔT also serves as the characteristic temperature scale. Using these characteristic length, time and temperature scales, we rescale the dimensional starred variables to yield

$$\Psi = \frac{\psi^*}{g_0 \alpha \Delta T D^3/\nu}, \quad \Theta = \frac{\Theta^*}{\Delta T},$$

where Ψ, Θ, and t are the dimensionless streamfunction, temperature and time respectively. The following dimensionless groups arise in the equation: Ra, Pr and Ω, defined previously and ϵ, the scale of the modulation. The Grashof number is defined as $Gr = Ra/Pr$.

We set up a coordinate system with the origin on the left (hot) wall. The sense of the (horizontal) x-axis is positive from left to right, and the vertical y-axis is positive from bottom to top. Using this coordinate system and the dimensionless variables defined above, the full Boussinesq equations for the transport of vorticity and energy written in streamfunction form are given by

$$\left.\begin{aligned} Gr\{\partial_t \nabla^2 \Psi + J(\Psi, \nabla^2 \Psi)\} &= \nabla^4 \Psi - \partial_x \Theta, \\ Ra\{\partial_t \Theta + J(\Psi, Y)\} &= \nabla^2 \Theta, \end{aligned}\right\} \tag{2}$$

where $J(u,v) = u_y v_x - u_x v_y$. The boundary conditions for the streamfunction and temperature are

$$\left.\begin{aligned} \Psi(0,y,t) = \Psi(1,y,t) = 0 = \Psi_x(0,y,t) = \Psi_x(1,y,t), \\ \Theta(0,y,t) = \tfrac{1}{2} + \tau_B y, \quad \Theta(1,y,t) = -\tfrac{1}{2} + \tau_B y, \end{aligned}\right\} \tag{3}$$

where $\tau_B = S/(\Delta T/D)$, and is the fifth dimensionless group that defines the problem. We find a relationship between the imposed vertical temperature stratification and the aspect ratio of the cavity by appealing to the asymptotic results of Gill (1966) who

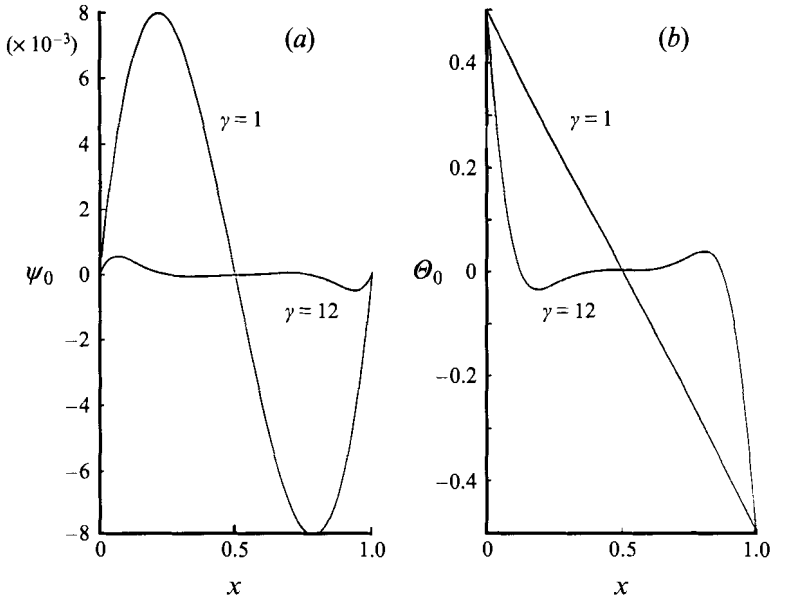

FIGURE 2. (*a*) Temperature and (*b*) velocity of the base state for $\gamma = 1, 12$.

showed that in the boundary-layer regime, the core stratification of the cavity is related to the aspect ratio by

$$\tau_B = 0.5/A. \tag{4}$$

Thus for a cavity of given aspect ratio, an equivalent slot problem can be constructed for $Ra \gg 1$.

2.1. *Parallel-flow solutions*

Equations (2) admit a steady parallel-flow solution. Thus seeking solutions of the type $\Psi = \Psi_0(x)$ and $\Theta = \Theta_0(x) + \tau_B y$ in (2) we obtain

$$\Psi_0^{\mathrm{iv}} - \Theta_0' = 0, \quad \Theta_0'' + Ra\,\tau_B \Psi_0' = 0,$$

where we have used primes to denote derivatives with respect to x. The boundary conditions become

$$\Psi_0(0) = \Psi_0(1) = 0 = \Psi_{0_x}(0) = \Psi_{0_x}(1),$$
$$\Theta_0(0) = 1, \quad \Theta_0(1) = 0.$$

Let $\Psi_0' = -v$ above; then the above two equations can be combined giving

$$v^{\mathrm{iv}} + 4\gamma^4 v = 0, \tag{5}$$

where $\gamma^4 = \frac{1}{4}\tau_B Ra$. This equation, proposed and solved by Elder (1965) has the solution (as given by Bergholz 1978)

$$v = Re\left[\frac{-\mathrm{i}}{8\gamma^2}\{f_1(x) - f_{-1}(x)\}\right],$$
$$\Theta_0 = Re\left[-\tfrac{1}{4}\{f_1(x) + f_{-1}(x)\}\right],$$

where

$$f_m(x) = \frac{\sinh[(1+m\mathrm{i})\gamma x] - \sinh[(1+m\mathrm{i})\gamma(1-x)]}{\sinh[(1+m\mathrm{i})\gamma]}.$$

We note that the sole remaining parameter in the equations is γ. How do the velocity and temperature profiles depend on γ? This is shown in figure 2 for $\gamma = 1, 12$. As can

be seen, for low γ the heat transfer is dominated by conduction (hence the nearly linear temperature profile). At larger values of γ most of the lateral temperature gradients exist only in a small region close to the walls, forming boundary layers. Since the velocity fields are set up by vorticity production due to thermal gradients, the velocity profiles also show a similar behaviour.

2.2. *Stability of the parallel flow*

This steady laminar flow becomes unstable when Gr is high enough. The stability of the steady parallel-flow solutions given by Ψ_0, Θ_0 can be examined in the usual way by considering the evolution of (small) superimposed disturbances which we denote as Ψ_D, Θ_D. Therefore the total flow field, which is the sum of the base flow and the superposed disturbances, is given as

$$\begin{bmatrix}\Psi(x,y,t)\\ \Theta(x,y,t)\end{bmatrix}=\begin{bmatrix}\Psi_0(x)\\ \Theta_0(x)+\tau_B y\end{bmatrix}+\begin{bmatrix}\Psi_D(x,y,t)\\ \Theta_D(x,y,t)\end{bmatrix}. \tag{6}$$

Substituting this expansion in (2) and linearizing, we get the following equations for the disturbance quantities:

$$\left.\begin{aligned} Gr\left\{\partial_t\nabla^2\Psi_D - v\frac{\partial\nabla^2\Psi_D}{\partial y}+v''\frac{\partial\Psi_D}{\partial y}\right\} &= \nabla^4\Psi_D-\partial_x\Theta_D,\\ Ra\left\{\partial_t\Theta_D - v\frac{\partial\Theta_D}{\partial y}+\Theta_0'\frac{\partial\Psi_D}{\partial y}-\tau_B\frac{\partial\Psi_D}{\partial x}\right\} &= \nabla^2\Theta_D,\end{aligned}\right\} \tag{7}$$

where $\Psi_0' = -v$ as before and $\nabla^2\Psi_0 = -v'$. These are subject to the boundary conditions

$$\Psi_D(0,y,t)=\Psi_D(1,y,t)=0=\Psi_{Dx}(0,y,t)=\Psi_{Dx}(1,y,t),$$
$$\Theta_D(0,y,t)=0,\quad \Theta_D(1,y,t)=0.$$

These linear disturbance equations can be subjected to suitable normal-mode analysis to give the stability behaviour of the slot. Therefore, seeking travelling wave solutions of the form

$$\begin{bmatrix}\Psi_D(x,y,t)\\ \Theta_D(x,y,t)\end{bmatrix}=\begin{bmatrix}\xi_\Psi(x)\\ \xi_\Theta(x)\end{bmatrix}e^{i(ky+\lambda t)}$$

gives equations identical to Bergholz (1978) which are written as

$$i\lambda \boldsymbol{B}_k V_\xi + \boldsymbol{H}_k V_\xi = 0, \tag{8}$$

where

$$\boldsymbol{B}_k=\begin{bmatrix}Gr\nabla_k^2 & 0\\ 0 & Ra\end{bmatrix}, \tag{9}$$

$$\boldsymbol{H}_k=\begin{bmatrix}(-ikv\nabla_k^2+ikv'')Gr-\nabla_k^4 & \partial_x\\ (ik\Theta_0'-\tau_B\partial_x)Ra & -ikRa\,v-\nabla_k^2\end{bmatrix}, \tag{10}$$

$$V_\xi=\begin{bmatrix}\xi_\Psi(x)\\ \xi_\Theta(x)\end{bmatrix},$$

where we have used $\nabla_k^2=\partial_{xx}-k^2$. The boundary conditions are

$$\left.\begin{aligned}\xi_\Psi=\xi_\Psi'=0,\quad x=0,1,\\ \xi_\Theta=0,\quad x=0,1.\end{aligned}\right\} \tag{11}$$

Investigator	*Pr*	*A*	Expt. Gr_c	Model Gr_c
Elder (1965)	1000	19	3.3×10^2	3.4×10^2
Vest & Arpaci (1969)	0.71	33.33	8.7×10^3	8.9×10^3
Hart (1971)	6.7	25	1.9×10^4	1.2×10^4

TABLE 2. A comparison of experimentally observed critical Gr_c with predictions of the model problem.

If k is assumed real and given, equations (8)–(11) can be solved as an eigenvalue problem in λ with $\mathrm{Re}[\mathrm{i}\lambda] > 0$ yielding growing solutions.

The stability of the slot flow has been extensively investigated by Bergholz (1978), who also provides references to much of the earlier work with the model. Experimental evidence for instability in tall cavities suggests the existence of both travelling and stationary modes (Elder 1965). Bergholz (1978), among others including Mizushima & Gotoh (1976) and Iyer (1973), explored these instability modes via numerical solution of equations (8)–(11), where *Gr* acts as a bifurcation parameter. We thus seek solutions in the parameter space *Pr*, γ, k. The critical *Gr* so obtained is minimized over all k, yielding Gr_c, the minimum critical *Gr* over all possible wavenumbers. We thus need to explore the solutions in the parameter space *Pr*, γ. Bergholz (1978) shows that solutions to equations (8)–(11) yield two competing modes: a travelling mode, driven by shear at low *Pr* and by buoyancy when *Pr* is large; and a stationary mode. At low *Pr*, the travelling mode dominates when γ is large, but at high *Pr* the travelling mode is dominant when γ is small. Thus there is a critical value γ_c for any given *Pr* when the instability type changes from travelling to stationary mode. The success of the model in accounting for the stability behaviour of tall cavities is shown in table 2 (taken from Bergholz 1978), where the critical *Gr* is tabulated for the onset of instability from the model (as given by (8)) together with the experimentally obtained values of the critical *Gr* by Elder (1965), Vest & Arpaci (1969) and Hart (1971). As can be seen the agreement is excellent.

2.3. *Solution to the eigenvalue problem*

Equations (8)–(11) have been solved numerically by standard second-order finite differences. The resulting system of equations yields a generalized algebraic eigenvalue problem that has been solved by well-known techniques (Moler & Stewart 1973). The accuracy of the solutions has been verified by mesh refinement. In this subsection we describe the solutions of equations (8)–(11), with special reference to long-wave solutions which will be found (in §3) to have a special significance for the model slot problem when the gravity is modulated.

While Bergholz (1978) has made a distinction between stationary and travelling modes of instability, we have found not one, but two types travelling modes: shear or buoyancy driven travelling modes as he describes, and modes that describe internal wave type of motion in the centre of the slot. Figure 3 shows the numerically computed eigenvalue spectrum for the case $Pr = 0.73$; $\gamma = 12$; $k = 3.52$; $Gr = 700.9 \times 10^3$. For this choice of parameters, $\tau_B = 0.16$. The real part of the eigenvalue (on the x-axis) is plotted versus the imaginary (oscillating) part. As can be seen all eigenvalues have negative real parts and are thus all damped. The dominant mode is given by a pair of complex-conjugate eigenvalues with extremely small (-10^{-6}) real part and hence very nearly approximates a neutral mode close to the bifurcation point. The first subdominant mode sits on the real axis and thus represents a stationary mode.

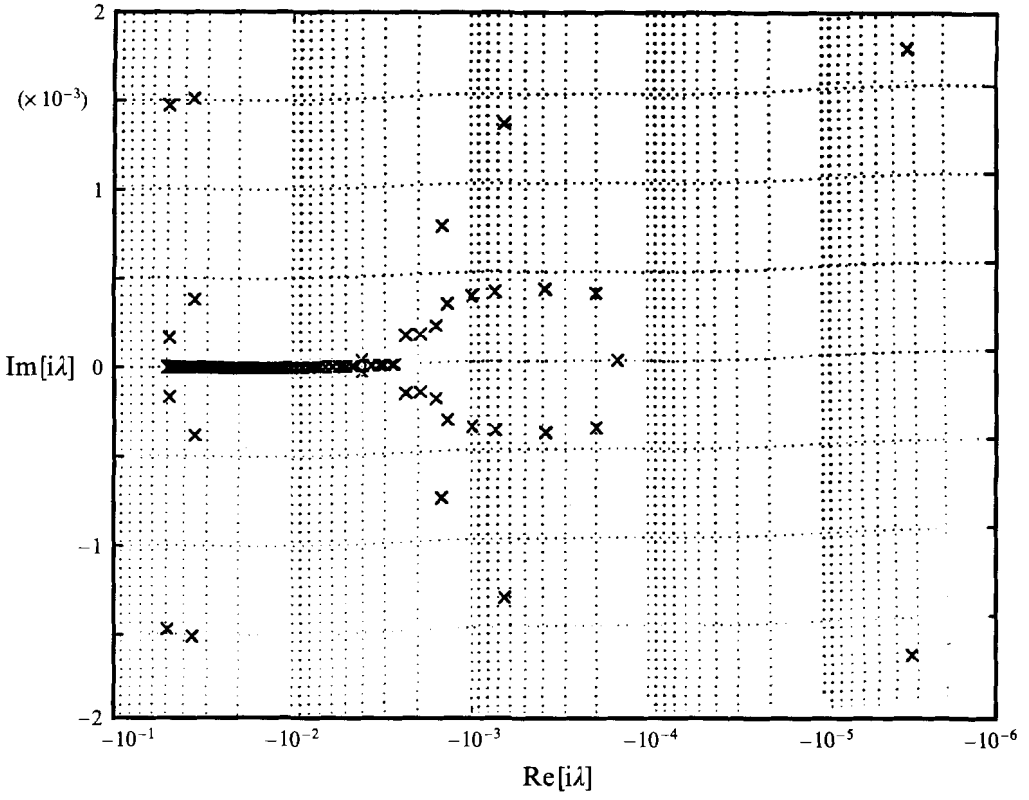

FIGURE 3. The eigenvalue spectrum, $\gamma = 12$, $Pr = 0.73$, $Gr = 700.9 \times 10^3$, $\tau_B = 0.16$, $k = 3.52$.

However, in figure 3 we find also a number of other travelling modes which, far from being randomly distributed, all fall in a rather neatly formed 'pitchfork' pattern. The 'handle' of the pitchfork consists of the real axis and the modes lying on it are stationary modes of zero frequency. As we move from left to right along any one of the two 'prongs' of the pitchfork, we encounter modes of decreasingly small damping, while the frequency rises and reaches a maximum value. We will now present a scaling argument to show that the modes that lie on this patchfork pattern are internal wave modes and this maximum value of frequency is the Brunt–Väisälä frequency. We remark that the argument is only valid because the internal wave modes can have a frequency no higher than the Brunt–Väisälä frequency. Thus we consider that the most weakly damped of these modes (which we will henceforth call the least-damped IW mode or simply the IW mode) has an eigenvalue the imaginary part of which is $\approx 3.935 \times 10^{-4}$. Casting the Brunt–Väisälä formula for the frequency N of linear waves in an infinite quiescent stratified medium in our scaling we obtain

$$N = \frac{2\gamma^2}{Pr^{1/2}\, Gr}. \tag{12}$$

Substituting the parameters for the test case given by figure 3 in the above formula we obtain $N = 4.809 \times 10^{-4}$. As can be seen this is in agreement with the frequency obtained by solving the full eigenvalue problem and leads to strong suspicion that these modes are indeed internal wave modes. This is confirmed by considering other cases, where again the frequency of the least-damped IW mode shows exactly the same

Test case parameters	Freq. from (8)–(11)	Ratio	Brunt–Väisälä frequency
$\gamma = 12$; $Pr = 0.73$ $k = 3.52$; $Gr = 700.9 \times 10^3$	4.8092×10^{-4}	1	3.9352×10^{-4}
$\gamma = 12$; $Pr = 0.73$ $k = 3.52$; $Gr = 350.45 \times 10^3$	9.6184×10^{-4}	2	7.958×10^{-4}
$\gamma = 12$; $Pr = 2.92$ $k = 3.52$; $Gr = 700.9 \times 10^3$	2.4046×10^{-4}	$\frac{1}{2}$	1.8387×10^{-4}
$\gamma = 16.97$; $Pr = 0.73$ $k = 3.52$; $Gr = 700.9 \times 10^3$	9.6174×10^{-4}	2	7.858×10^{-4}

TABLE 3. The frequencies of the IW wave modes as predicted by the eigenvalue problem compared with the Brunt–Väisälä formula for linear waves. The third column shows the ratio of the frequency with 4.8092×10^{-4}, thus clarifying the scaling behaviour.

scaling in γ, Pr, Gr as equation (12) requires. This is shown in table 3 where the frequency of the internal wave modes as given by equations (8)–(11) is compared to (12). In row 1 we show the case mentioned previously, with $Pr = 0.73$, $\gamma = 12$, $Gr = 7.009 \times 10^5$, $k = 3.52$, and the frequencies obtained by the two methods, namely solving the full eigenvalue problem (3.935×10^{-4}) and using the Brunt–Väisälä frequency (4.809×10^{-4}), are also noted. To study the scaling behaviour of the frequencies we have reduced the value of Gr by a factor of $\frac{1}{2}$ in row 2 of table 3, and both the frequencies double, consistent with the Brunt–Väisälä formula. Similarly in rows 3 and 4 we have examined the scaling with respect to Pr and γ and have found the behaviour to be consistent with (12). This offers convincing evidence that the modes in question are indeed IW modes.

The reason for the agreement between the frequencies predicted by (8)–(11) and (12) is made quite clear by considering the main equations (8)–(11) in the limit of large γ (when boundary layers form): the base velocity and its gradients are non-zero only in a small boundary layer close to the wall, thus outside the boundary layer, $v(x) = 0 = v''(x)$. Similarly temperature gradients are zero outside the boundary layer, leading to $\Theta_D'(x) = 0$. These vanishing velocity and thermal gradients outside the boundary layer imply that the diffusion of heat and vorticity can be ignored in the core. With the above-mentioned approximations, (8)–(11) can be reduced to a single equation (of higher order) in which N reappears:

$$\partial_{tt} \nabla_k^2 \Psi_D + N^2 \partial_{xx} \Psi_D = 0. \tag{13}$$

This equation governs inviscid internal waves in a quiescent medium. It yields travelling wave solutions of frequency N, which explains the agreement previously noted in table 3.

The eigenvalue spectrum shown in figure 3 depends on four parameters: Pr, τ_B, k and Gr. We now investigate the nature of the spectrum as the core stratification of the cavity is varied. In figure 4 we show the eigenvalue spectrum for $\tau_B = 0.05, 0.01$, while holding the other parameters fixed. As the stratification becomes weaker the internal wave modes tend to weaken and disappear. This can be understood by looking into the mechanism by which the IW are set up. If an isotherm is titled (slightly), the stable density gradient tries to restore it, but it overshoots and sets up a travelling wave. Hence the effect of weakening the stratification is to reduce the strength of the restoring force and this tends to destroy the waves. The effect of Pr can also be understood in similar terms. Keeping Gr and γ fixed, τ_B is given as $\tau_B = 4\gamma^4/(Gr\,Pr)$. Thus for large Pr, τ_B decreases, destroying the IW modes.

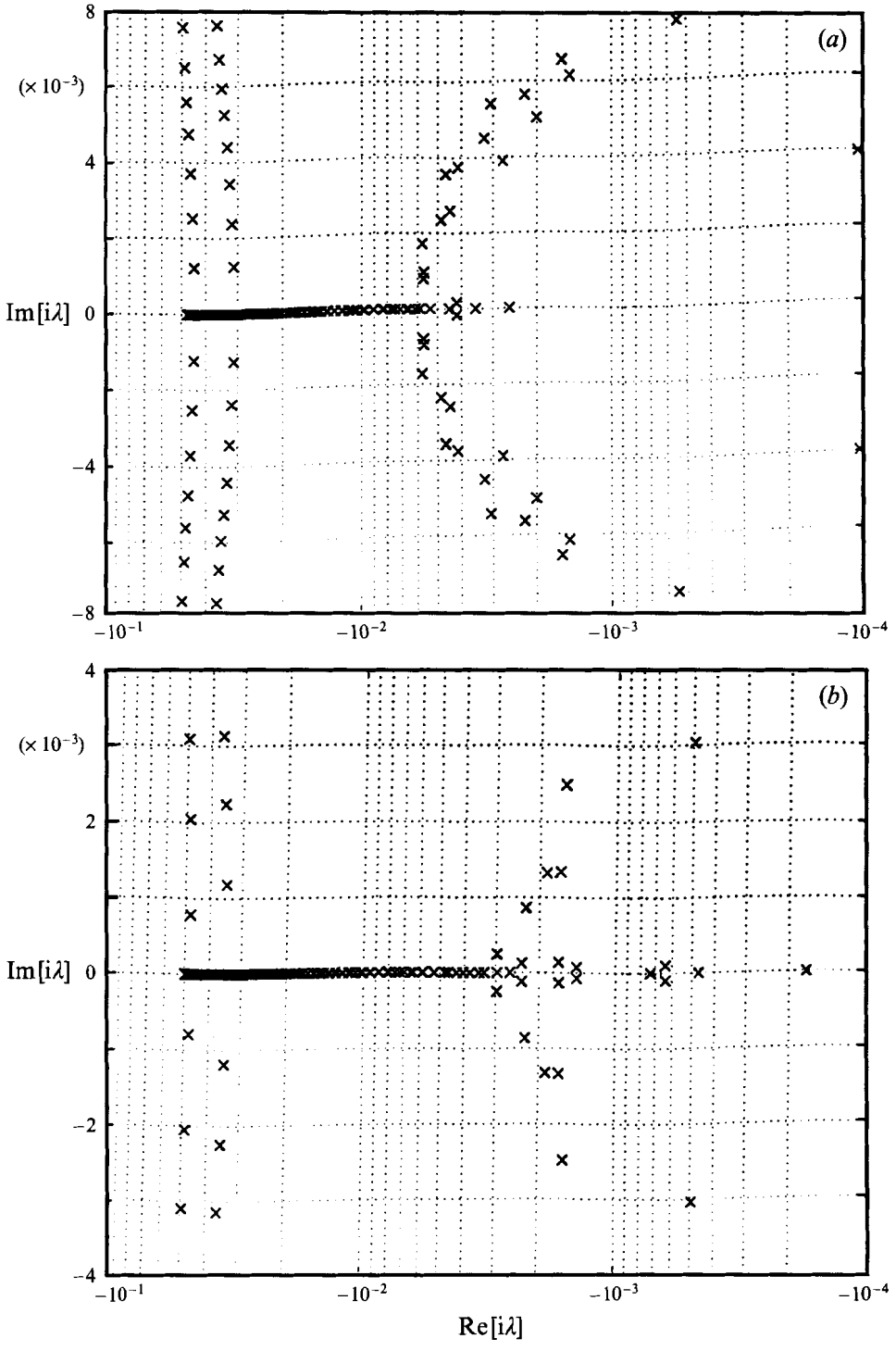

FIGURE 4. Eigenvalue spectrum as the stratification is varied for $\gamma = 12$, $Pr = 0.73$, $Gr = 700.9 \times 10^3$ and $k = 3.52$. (*a*) $\tau_B = 0.01$, the Brunt–Väisälä frequency is 2.670×10^{-4}. (*b*) $\tau_B = 0.05$, the Brunt–Väisälä frequency is 1.194×10^{-4}.

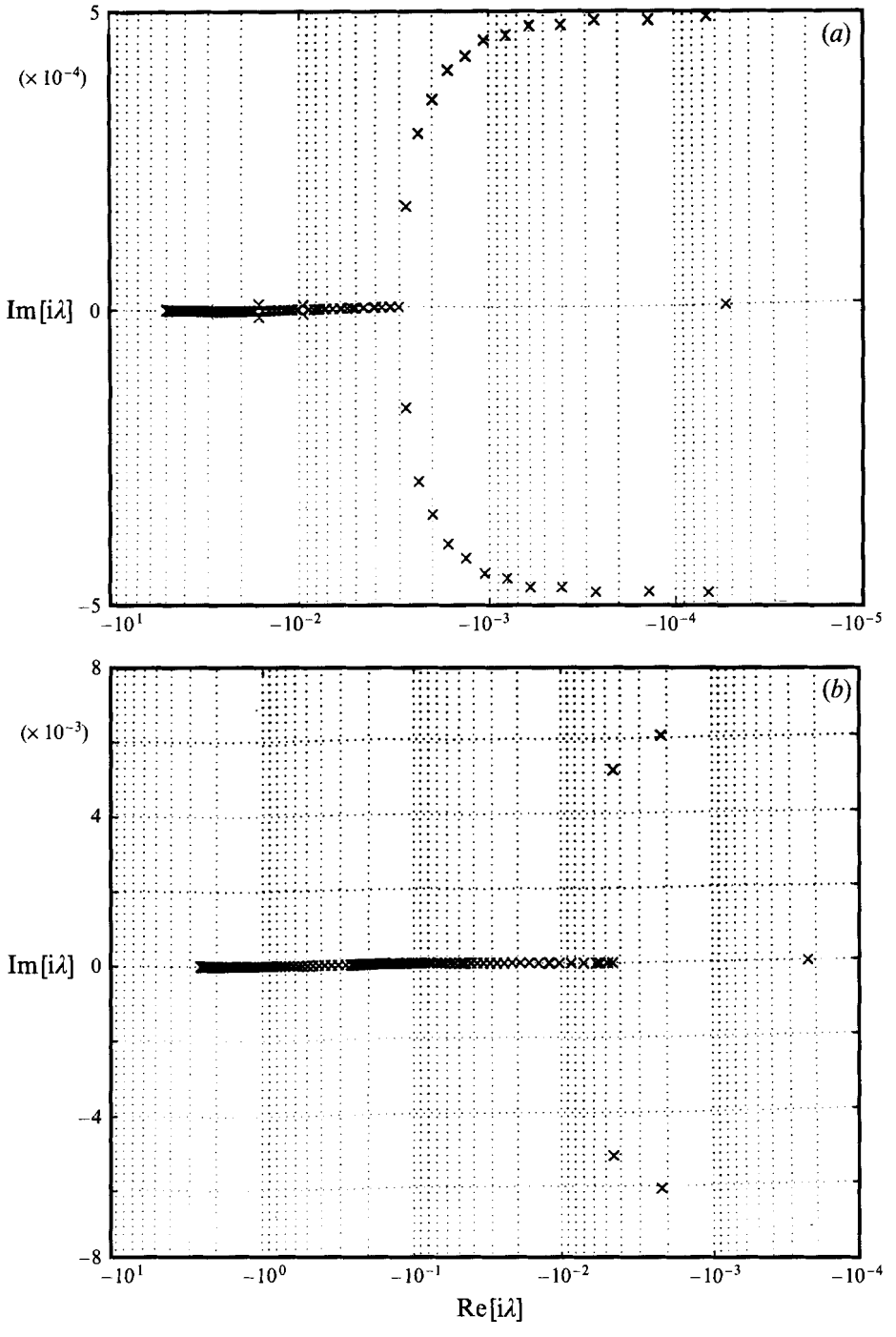

FIGURE 5. The spectra corresponding to (*a*) case I and (*b*) case II in the long-wave limit.

One final parameter is the axial wavenumber k. We will find in § 3 that the long-wave modes (corresponding to $k = 0$) are of particular relevance to the forced problem. Hence we show in figure 5 the eigenvalue spectra for two different Pr: case I $Pr = 0.73$, $Gr = 700.9 \times 10^3$, $\gamma = 12$, $\tau_B = 0.16$, $k = 0$, and case II $Pr = 10$, $Gr = 10^4$, $\gamma = 10$,

$\tau_B = 0.4$, $k = 0$. In both cases the dominant mode is a stationary mode; however the frequency of the least-damped travelling mode compares extremely well with the Brunt–Väisälä frequency ($N = 4.809 \times 10^{-4}$ for case I and $N = 6.3 \times 10^{-3}$ for case II), indicating that they are internal waves. This is important because it shows that the only travelling modes to survive in the long-wave limit are IW modes.

3. The effect of small-amplitude modulation: resonances

In this section we will examine the infinite-slot problem when the gravity is modulated, but the amplitude of the modulation, ϵ, is small. The full governing equations for the gravity-modulated problem are given by

$$\begin{aligned} Gr\{\partial_t \nabla^2 \Psi + J(\Psi, \nabla^2 \Psi)\} &= \nabla^4 \Psi - \partial_x \Theta\{1 + \epsilon \cos \Omega t\}, \\ Ra\{\partial_t \Theta + J(\Psi, \Theta)\} &= \nabla^2 \Theta. \end{aligned} \tag{14}$$

In the limit of small ϵ we seek perturbation solutions to (14):

$$\begin{bmatrix} \Psi(x,y,t) \\ \Theta(x,y,t) \end{bmatrix} = \begin{bmatrix} \psi_0(x) \\ \theta_0(x) + \tau_B y \end{bmatrix} + \epsilon \begin{bmatrix} \psi_1(x,y,t) \\ \theta_1(x,y,t) \end{bmatrix} + \epsilon^2 \begin{bmatrix} \psi^2(x,y,t) \\ \theta_2(x,y,t) \end{bmatrix} + \ldots. \tag{15}$$

At $O(\epsilon^0)$ we recover the base-flow solutions given in the previous section. At $O(\epsilon)$ we get the equations

$$\left.\begin{aligned} Gr\left\{\partial_t \nabla^2 \psi_1 - v \frac{\partial \nabla^2 \psi_1}{\partial y} + v'' \frac{\partial \psi_1}{\partial y}\right\} &= \nabla^4 \psi_1 - \partial_x \theta_0 \cos \Omega t - \partial_x \theta_1, \\ Ra\left\{\partial_t \theta - v \frac{\partial \theta_1}{\partial y} + \theta_0' \frac{\partial \psi_1}{\partial y} - \tau_B \frac{\partial \psi_1}{\partial x}\right\} &= \nabla^2 \theta_1, \end{aligned}\right\} \tag{16}$$

subject to the boundary conditions

$$\begin{gathered} \psi_1(0,y,t) = \psi_1(1,y,t) = 0 = \psi_{1x}(0,y,t) = \psi_{1x}(1,y,t), \\ \theta_1(0,y,t) = 0; \quad \theta_1(1,y,t) = 0. \end{gathered}$$

We note that since (16) is linear, and the buoyancy term $\partial_x \theta_0 \cos \Omega t$ is a function of x alone, equations (16) admit parallel-flow solutions of the form

$$\psi_1 = \psi_1(x,t), \theta_1 = \theta_1(x,t),$$

giving,

$$\partial_t \boldsymbol{B}_0 \boldsymbol{V}_1 + \boldsymbol{H}_0 \boldsymbol{V}_1 = \boldsymbol{F}_1 \cos \Omega t, \tag{17}$$

where B_0 and H_0 are obtained by setting $k = 0$ in the definitions for $\boldsymbol{B}_k$ and $\boldsymbol{H}_k$, equations (9) and (10), and

$$\boldsymbol{V}_1 = \begin{bmatrix} \psi_1(x,t) \\ \theta_1(x,t) \end{bmatrix}, \quad \boldsymbol{F}_1 = \begin{bmatrix} -\partial_x \theta_0 \\ 0 \end{bmatrix}.$$

For the long-wave approximation ($k = 0$) equation (17) is a real-valued equation, and hence it is possible to solve it by the method of complex embedding. We therefore set

$$\boldsymbol{V}_1 = Re[\bar{\boldsymbol{V}}_1 e^{i\Omega t}], \quad \bar{\boldsymbol{V}}_1 = \begin{bmatrix} \bar{\psi}_1(x) \\ \bar{\theta}_1(x) \end{bmatrix}$$

in equation (17) giving

$$(i\Omega B_0 + H_0)\, \bar{\boldsymbol{V}}_1 = \boldsymbol{F}_1; \tag{18}$$

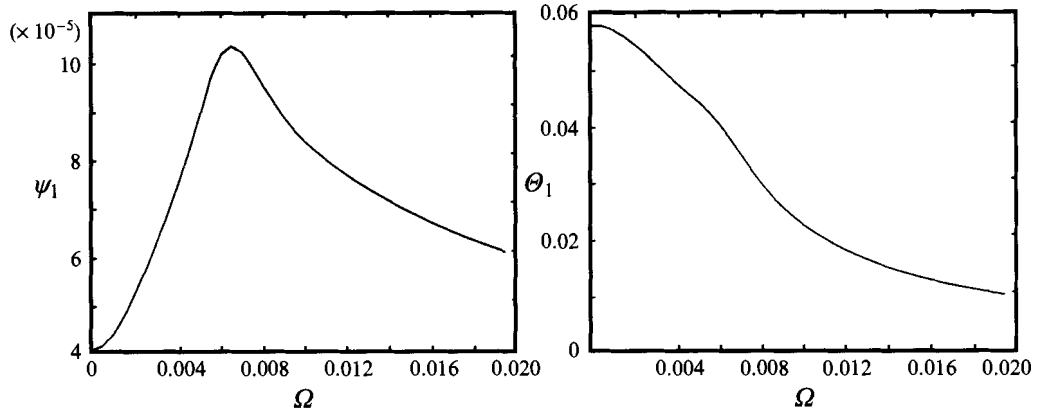

FIGURE 6. The frequency–amplitude response curves for streamfunction and temperature fields at $O(\epsilon)$.

$\bar{\psi}_1(x)$ and $\bar{\theta}_1(x)$ denote the response amplitude. Thus we see that the solutions to the forced problem given by (18) are intimately related to the long-wave ($k = 0$) modes of the eigenvalue problem, (8)–(11). In the previous section we have seen that in the long-wave limit the IW modes are the only travelling modes to survive. It should be possible to excite them in the context of equation (18). This is what has been seen by Farooq & Homsy (1994) with reference to a cavity of aspect ratio unity. Consider figure 6 which shows the frequency–amplitude response curve for case II of the previous section. The maximum value of the streamfunction and temperature (over the domain) have been plotted versus the driving frequency Ω. As can be seen we get a resonant response for the streamfunction when $\Omega \approx 6.0 \times 10^{-3}$ (note that the numerically computed eigenfrequency of the dominant mode IW was 6.065×10^{-3}). The response of the temperature field does not show any resonances and goes to zero asymptotically as the driving frequency becomes large. One interesting point to be noted is that no evidence of any excitation of the stationary modes when $\Omega = 0$ was found.

Thus we see that the slot problem under gravity modulation produces resonances with natural modes of the system. This will be the basis of our study of the effect of larger-amplitude modulation, which is the subject of the next section.

4. Effect of modulation when $\varepsilon \sim O(1)$: parametric instability

Investigations of the stability of time-dependent fluid systems have mainly focused on sinusoidal time variation of three classes of flows: parallel shear flows, buoyancy-driven flows, and centrifugally driven (Rossby) flows. In the first category work has been done on the stability of Stokes layers (Kerczek & Davis 1974). They consider infinitesimal two-dimensional disturbances and find that the flow is stable even at very large values of a characteristic Reynolds number based on the frequency of oscillation, and the Stokes-layer thickness in agreement with experimental evidence. However Kerczek & Davis (1976) while considering the stability of a slot with density stratification in which the flow is driven by an oscillating wall (as compared to an oscillating buoyant force as in our case) found that the flow can be destabilized under suitable conditions of oscillation amplitude and frequency. This is similar to Gresho & Sani (1970) who consider the stability of a horizontal layer of fluid heated from above or below for the case of a time-dependent buoyancy force which is generated by shaking the fluid layer. They too find that statically stable eigenmodes of the

Rayleigh–Bénard problem can be made unstable by suitably choosing the modulation amplitude and frequency. Work on modulated Couette and Rossby flows has been reviewed by Davis (1976).

Despite the range of geometries and operative mechanisms involved in all these classes of problems, the following general picture hold true: proper choice of the amplitude and frequency of the modulation can lead to dramatic modification in behaviour of the flow, resulting in dynamic destabilization of stable systems, or vice versa.

There is a remarkable similarity between the modal dynamics of these infinite-dimensional systems and a simple pendulum with modulated pivoting, as first pointed out by Gresho & Sani (1970). The latter problem is governed by the Mathieu equation (see Stoker 1950), for which it can be shown via Floquet theory that for the right choice of modulation frequency and amplitude, unstable hyperbolic points for the unmodulated problem become attracting limit cycles, and stable centres yield unstable cycles (with hyperbolic Poincaré sections).

In this section we examine the effect of buoyancy modulation on the eigenspectrum of the steady problem which we have computed in §2. The most relevant dynamics of the linear problem are governed by the most-dangerous eigenmode. Hence we construct a finite Galerkin projection of the full nonlinear operator on the spectral eigenmodes of the linearized operator. This leads to a truncated system of dynamical equations that governs the temporal evolution of the modes under excitation.

4.1. *Mathematical formulation*

We consider the infinite-slot geometry defined previously. The full equations are (again)

$$\left.\begin{aligned} Gr\{\partial_t \nabla^2 \Psi + J(\Psi, \nabla^2 \Psi)\} &= \nabla^4 \Psi - \partial_x \Theta\{1 + \epsilon \cos \Omega t\}, \\ Ra\{\partial_t \Theta + J(\Psi, \Theta)\} &= \nabla^2 \Theta. \end{aligned}\right\} \tag{19}$$

We have seen from the linearized treatment of these equations in the previous section that parallel-flow solutions of this equation are relevant for the gravity-modulated problem. Our present concern will be to investigate the effect of finite amplitude of modulation. In the past we noted that the behaviour of the system for $\epsilon \ll 1$ were governed by the least-damped (or the most dominant) of the linear eigenmodes of the system.

We seek solutions to (19) by a Galerkin expansion using the eigenfunctions as trial and test functions. Since we know that the most relevant dynamics is (certainly in the small-ϵ limit) dominated by the most-dangerous mode, we propose a severely truncated Galerkin expansion where we retain only the most dominant mode. Hence we have

$$\left.\begin{aligned} \Psi &= \Psi_0(x) + B(t)\, \Psi_1(x, y) + \ldots, \\ \Theta &= \Theta_0(x) + \tau_B y + A(t)\, \Theta_1(x, y) + \ldots, \end{aligned}\right\} \tag{20}$$

where

$$\begin{bmatrix} \Psi_0(x) \\ \Theta_0(x) + \tau_B y \end{bmatrix}$$

is the parallel-flow (base state) solution to the constant-gravity problem, $\Psi_1(x, y)$ and $\Theta_1(x, y)$ are the partitioned (respectively streamfunction and temperature) components of the eigenfunction from (8), and $A(t)$ and $B(t)$ are the time-dependent coefficients that determine the temporal dynamics of the modes. The base state has been included in the expansion so that the problem behaviour should reduce to the earlier asymptotic

results in the limit of small ϵ. We have seen from the linearized treatment that the modes that 'see' the gravity modulation are the long-wave ($k = 0$) modes. Hence we choose $(\Psi_1(x,y), \Theta_1(x,y))$ to be the least-damped parallel-flow mode for any particular choice of Gr, Pr and τ_B. For $k = 0$, $\Psi_1 = \Psi_1(x)$ and $\Theta_1 = \Theta_1(x)$.

Substituting the expansion (20) into (19) we obtain

$$\left.\begin{aligned} Gr\,\dot{B}(t)\,\Psi_1'' &= \Psi_0^{\mathrm{iv}} + B(t)\,\Psi_1^{\mathrm{iv}} - (\Theta_0' + A(t)\,\Theta_1')(1+\epsilon\cos\Omega t), \\ Ra\,\dot{A}(t)\,\Theta_1 &= \tau_B\,Ra(\Psi_0 + B(t)\,\Psi_1) + \Theta_0'' + A(t)\,\Theta_1'', \end{aligned}\right\} \tag{21}$$

where primes denote derivatives with respect to x as before and dots denote derivatives with respect to time. Since Ψ_0 and Θ_0 satisfy (5), equations (21) simplify to

$$\left.\begin{aligned} Gr\,\dot{B}(t)\,\Psi_1'' &= B(t)\,\Psi_1^{\mathrm{iv}} - \epsilon\Theta_0'\cos\Omega t - A(t)\,\Theta_1'(1+\epsilon\cos\Omega t), \\ Ra\,\dot{A}(t)\,\Theta_1 &= \tau_B\,Ra\,B(t)\,\Psi_1' + A(t)\,\Theta_1''. \end{aligned}\right\} \tag{22}$$

Rearranging the second equation (22), we get

$$B(t)\,\Psi_1' = \frac{1}{\tau_B\,Ra}(Ra\,\dot{A}(t)\,\Theta_1 - A(t)\,\Theta_1'']). \tag{23}$$

Equation (23) can easily be manipulated to yield

$$\left.\begin{aligned} B(t)\,\Psi_1^{\mathrm{iv}} &= \frac{1}{\tau_B\,Ra}(Ra\,\dot{A}(t)\,\Theta_1''' - A(t)\,\Theta_1^{\mathrm{v}}), \\ \dot{B}(t)\,\Psi_1'' &= \frac{1}{\tau_B\,Ra}(Ra\,\ddot{A}(t)\,\Theta_1' - \dot{A}(t)\,\Theta_1'''). \end{aligned}\right\} \tag{24}$$

We can eliminate $B(t)$ and $\Psi_1(x)$ from (24) and (22) giving

$$\ddot{A}(t)\,\Theta_1 - \dot{A}\left(\frac{\Theta_1'''}{Ra} + \frac{\Theta_1'''}{Gr}\right) + A\left(\frac{\Theta_1^{\mathrm{v}}}{Gr\,Ra} + \frac{\Theta_1'\tau_B\cos\Omega t}{Gr}(1+\epsilon\cos\Omega t)\right) = -\epsilon\frac{\Theta_0'\tau_B\cos\Omega t}{Gr}. \tag{25}$$

Thus we have reduced two first-order ODEs in time to one of second order. Taking the Galerkin product in the usual way and defining

$$\left.\begin{aligned} &\Gamma_1 = \langle\Theta_1', \Theta_1'\rangle, \quad \Gamma_2 = \langle -\Theta_1''', \Theta_1'\rangle\frac{1+Pr}{Ra}, \\ &\Gamma_3 = \langle\Theta_1^{\mathrm{v}}, \Theta_1'\rangle\frac{1}{Gr\,Ra}, \quad \Gamma_4 = \langle\Theta_1', \Theta_1'\rangle\frac{1}{Gr}, \quad \Gamma_5 = \langle\Theta_0', \Theta_1'\rangle\frac{\tau_B}{Gr}, \end{aligned}\right\} \tag{26}$$

where we define the inner product as

$$\langle a, b\rangle = \int_0^1 ab^*\,\mathrm{d}x, \tag{27}$$

where the asterisk denotes the complex conjugate, (25) assumes the form

$$\ddot{A}(t)\,\Gamma_1 + \dot{A}\Gamma_2 + A(\Gamma_3 + \Gamma_4(1+\epsilon\cos\Omega t)) = -\epsilon\Gamma_5\cos\Omega t. \tag{28}$$

Dividing through by Γ_1 and introducing the new variable

$$\epsilon u = \frac{A}{\Gamma_5/\Gamma_1} \tag{29}$$

we get the following equation:

$$\ddot{u}(t)+\dot{u}\frac{\Gamma_2}{\Gamma_1}+u\left(\frac{\Gamma_3}{\Gamma_1}+\frac{\Gamma_4}{\Gamma_1}(1+\epsilon\cos\Omega t)\right)=-\cos\Omega t. \tag{30}$$

If we rescale time as $\Omega t=\tau$ equation (30) becomes

$$\Omega^2 u_{\tau\tau}+u_\tau\frac{\Gamma_2\Omega}{\Gamma_1}+u\left(\frac{\Gamma_3}{\Gamma_1}+\frac{\Gamma_4}{\Gamma_1}(1+\epsilon\cos\tau)\right)=-\cos\tau. \tag{31}$$

We recall that λ is the eigenvalue obtained from (8)–(11); thus its real part, λ_R, denotes the frequency of the eigenmode. We introduce the detuning parameter, σ, defined by $\Omega=\sigma\lambda_R$. Equation (31) then yields

$$u_{\tau\tau}+u_\tau\frac{\mu_1}{\sigma}+u(\mu_2+\mu_3(1+\epsilon\cos\tau))\frac{1}{\sigma^2}=-\frac{1}{\lambda_R^2\sigma^2}\cos\tau, \tag{32}$$

where

$$\mu_1=\frac{\Gamma_2}{\Gamma_1}\frac{1}{\lambda_R},\quad \mu_2=\frac{\Gamma_3}{\Gamma_1}\frac{1}{\lambda_R^2},\quad \mu_3=\frac{1}{\lambda_R^2 Gr}. \tag{33}$$

One final transformation brings the equation into the desired form: putting

$$u=\eta(\tau)\exp\left(-\frac{\mu_1}{2\sigma}\tau\right) \tag{34}$$

which allows us to write (32) as

$$\eta_{\tau\tau}+\frac{1}{\sigma^2}(\mu_2+\mu_3-\tfrac{1}{4}\mu_1^2+\epsilon\mu_3\cos\tau)\eta=-\exp\left(\frac{\mu_1}{2\sigma}\tau\right)\frac{1}{\lambda_R^2\sigma^2}\cos\tau. \tag{35}$$

We note that (35) has the form of a Mathieu equation. Hence its behaviour can be investigated by Floquet theory.

4.2. *Solution of the Mathieu equation: Floquet theory*

Floquet theory can be brought to bear on equation (35), the homogeneous form of which we cast in the form of the standard Hill's equation:

$$\eta_{\tau\tau}+\frac{1}{\sigma^2}Q(\tau)\eta=0, \tag{36}$$

where $Q(\tau)=\mu_2+\mu_3-\frac{1}{4}\mu_1^2+\epsilon\mu_3\cos\tau$, and we note that $Q(\tau+2\pi)=Q(\tau)$. Floquet's theorem guarantees the existence of two normal solutions for (36). The normal solutions can be constructed as follows. Integrate (36) from 0 to 2π (numerically if necessary) with the following two sets of initial conditions:

$$\left.\begin{aligned}\eta_1(0)&=1;\quad \eta_1'(0)=0,\\ \eta_2(0)&=0;\quad \eta_2'(0)=1.\end{aligned}\right\} \tag{37}$$

Then the Floquet multiplier, $\sigma_{F_{1,2}}$ is given by the roots of the equation

$$\sigma_F^2-\sigma_F(\eta_1(2\pi)+\eta_2'(2\pi))+1=0 \tag{38}$$

and the Floquet exponents, $\chi_{F_{1,2}}$ are related to the Floquet multiplier through

$$\chi_{F_{1,2}}=\frac{\ln\sigma_{F_{1,2}}}{2\pi}. \tag{39}$$

$Gr = 10^4$; $Pr = 10$; $k = 0$; $\gamma = 10$
Eigenvalue: $i\lambda = -0.0021703 \pm 0.006065i$
$\mu_1 = 0.68836 - 0.00028i$
$\mu_2 = -0.12287 + 0.00111i$
$\mu_3 = 1.08740$

TABLE 4. The parameters of the first test case.

Furthermore, the theorem guarantees the existence of two normal solutions which form a fundamental set and can be written as

$$\eta(\tau) = N_1 \exp(\chi_{F_1}\tau) + N_2 \exp(\chi_{F_2}\tau), \tag{40}$$

where $N_1(\tau)$ and $N_2(\tau)$ are periodic with period 2π. We immediately see from (40) that if $\mathrm{Re}(\chi_{F_{1,2}}) > 0$, then $\lim_{\tau\to\infty} \eta(\tau) \to \infty$. If $Q(\tau)$ is a real-valued function, then $\eta_1(2\pi)$ and $\eta_2'(2\pi)$ are also real valued, implying that the roots of (38) are either real or complex conjugates. If the real part of the Floquet exponent is non-zero then we get growing solutions for the Hill's equation, a phenomenon called parametric resonance. (This is necessarily true, because if σ_{F_1} and σ_{F_2} are the two Floquet multipliers, $\sigma_{F_1}\sigma_{F_2} = 1$ from (38), implying $\chi_{F_1} = -\chi_{F_2}$, hence one of the exponential terms in (40) must grow.)

We begin by pointing out that since Ψ_1 and Θ_1 are complex-valued functions of x, the coefficients μ_1, μ_2, μ_3 in (35) are complex valued, implying that η in (40) is always a growing function of time. This can be proven for the case when $Q(\tau)$ is complex valued, see Magnus & Winkler (1966). However this does not necessarily mean that the mode is unstable since η is related to u through (34), using which in (40) we get

$$u = N_1 \exp\left(-\frac{\mu_1}{2\sigma}\tau + \chi_{F_1}\tau\right) + N_2 \exp\left(-\frac{\mu_1}{2\sigma}\tau + \chi_{F_2}\tau\right).$$

The condition for stability is thus given by

$$\mathrm{Re}\left[\chi_{F_{1,2}} - \frac{\mu_1}{2\sigma}\right] < 0. \tag{41}$$

Since $\chi_{F_{1,2}}$ are obtained by integrating the ODE over one period of oscillation, they are functions of ϵ. Thus it is necessary to investigate the dependence of χ_F on ϵ in order to determine the potential for parametric instability of (32). Therefore let us pick a test case, shown in table 4, corresponding to a travelling mode at $Pr = 10$. μ_1, μ_2 and μ_3 have been evaluated by (33). We proceed to construct the normal solutions for the Mathieu equation (35). A fourth-order Runge–Kutta method was employed to integrate the equations subject to the initial conditions (37). In doing this a choice has to be made for the values of σ and ϵ. Then the Floquet exponents can be evaluated from (38).

Let us fix the value of σ at 1 and look at the effect of ϵ on χ_F. In figure 7, the solid curve shows the real part of χ_F plotted as a function of ϵ. The dashed line shows the real part of $\mu_1/2\sigma$, which of course is independent of ϵ. The intersection of the two curves gives the critical ϵ, $\epsilon_c \approx 2.07$, for which we get growing solutions. Thus there is a critical ϵ_c below which the parallel-flow solutions are damped and above which they are unstable.

This has also been verified by full numerical simulation of the untransformed ODE, (32): setting $\sigma = 1$ and the parameters μ_1, μ_2, μ_3 as given in table 4 and integrating for a large interval of time, say a hundred oscillations of the forcing frequency (the

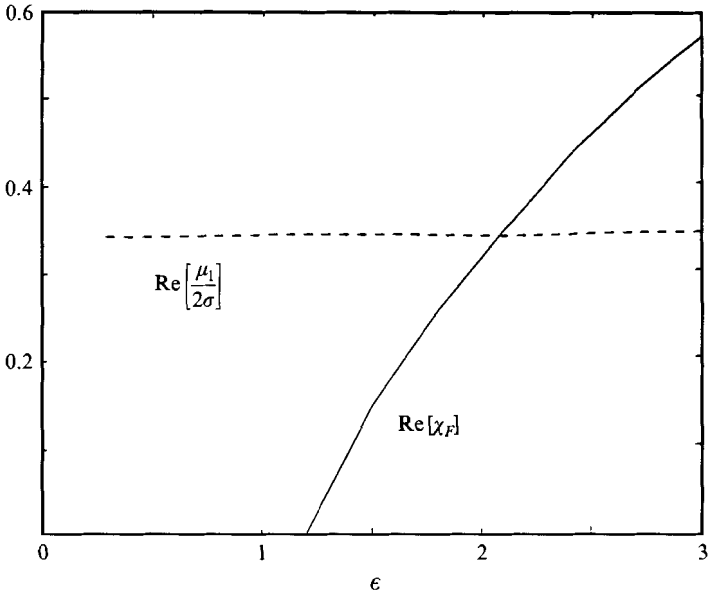

FIGURE 7. The real part of χ_F *vs.* ϵ, and its intersection with the real part of the $\mu_1/2\sigma$ curve.

integration is carried out using an accurate Runge–Kutta scheme as before), the solution either approaches steady oscillations or grows, depending on the choice of ϵ. The results are shown in table 5 where the nature of the solution, stable (S) or unstable (U), is displayed for various choices of ϵ. The table confirms the results of the Floquet theory and shows that for $\epsilon > 2.07$ we get growing solutions. The nature of the solution is further shown in figure 8 where (*a*) shows steady periodic oscillations and (*b*) shows growth due to parametric resonance.

Before we move on to investigate the effect of frequency of modulation on ϵ_c, we consider the effect of the choice of the eigenmode that is used as the basis of the expansion (20). We find that if a more strongly damped mode is used, then the instability threshold is higher: selecting a mode corresponding to the eigenvalue $\mathrm{i}\lambda = -0.0044 + 0.00513\mathrm{i}$, the coefficients of the evolution equation then are $\mu_1 = 1.80911 - 0.00652\mathrm{i}$, $\mu_2 = -0.5884 - 0.0508\mathrm{i}$, $\mu_3 = 1.5004$. The value of ϵ_c is calculated to be 3.41 and is higher than the value obtained earlier. This trend has been verified for other modes as well.

4.3. *Parametric dependence: effect of frequency, Prandtl number and stratification*

We have seen for the test cases studied that there exists a critical modulation amplitude, ϵ_c, above which the modulated parallel flow is unstable. We are interested in the dependence of this result on the parameters of the problem. We investigate the effect of the frequency of modulation, by considering the effect of changes in the detuning parameter, σ. The behaviour seen as $\sigma = 1$, i.e. existence of an ϵ_c above which the solutions are unstable, holds as σ is varied. Hence we repeat the calculations of the previous subsection for various σ and the results are shown in figure 9(*a*) which shows ϵ_c plotted as a function of σ. Generally speaking, the value of ϵ_c appears to increase at high σ indicating that high-frequency modulation is not very effective in producing parametric instabilities. The behaviour at lower σ is more complicated. The curve shows several maxima and minima. The minima occur at $\sigma \approx 1.6, 0.8, 0.55, 0.40, 0.325, 0.275, \ldots$. Note that the constant term in $Q(\tau)$ has real part, $Q_R = \mathrm{Re}\,[\mu_2 + \mu_3 - \mu_1^2/4] \approx$

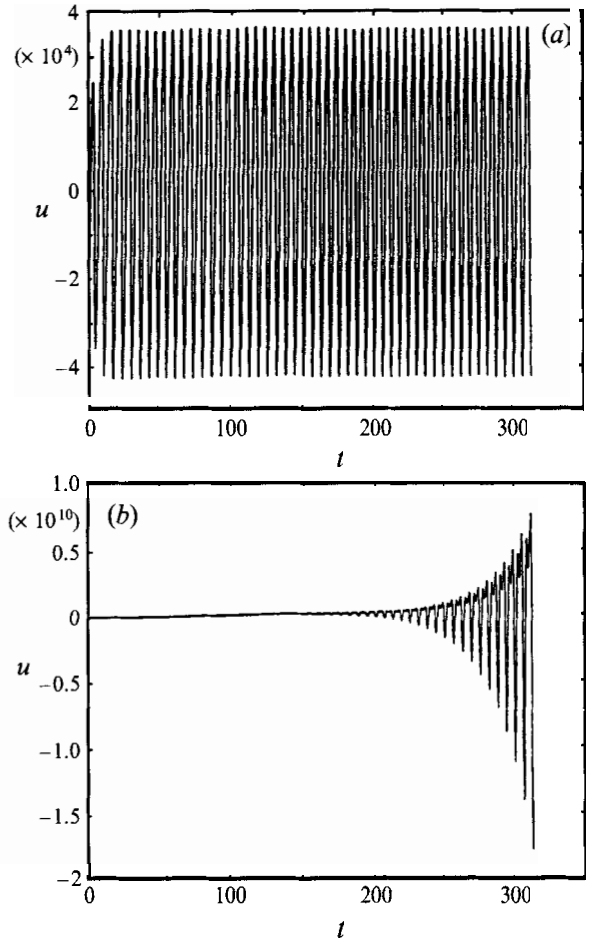

FIGURE 8. The effect of ϵ on the full Mathieu equation for $\epsilon = 0.3$ and $\epsilon = 2.2$ showing stable (S) and unstable (U) solutions by direct integration.

(*a*) ϵ	Nature of solution	(*b*) ϵ	Nature of solution
1.0	S	1.4	U
1.5	S	1.3	U
2.0	S	0.9	U
2.1	U	0.8	U
2.2	U	0.7	S

TABLE 5. The nature of solution, stable periodic oscillations (S) or growing unstable (U) solutions as ϵ is varied: (*a*) Full numerical simulation of (32); (*b*) full numerical simulation of (43).

0.8. Hence the minima seem to come at approximately $2Q_R$, Q_R, $\frac{2}{3}Q_R$, $\frac{1}{2}Q_R$, $\frac{2}{5}Q_R$ and $\frac{1}{3}Q_R$. Further we note that the lowest value of ϵ_c over all σ occurs at $\sigma \approx 1.7$ or $\approx 2Q_R$. It is remarkable that the minima should occur at simple rational fractions of Q_R, and this is almost certainly (though perhaps not simply) related to the well-known stability chart (not presented here) of the Mathieu equation. For small σ equation (35) becomes extremely stiff and hence we rely on the WKB method which is outlined in Appendix A. The result shows that for the limiting case of $\sigma \to 0$, $\epsilon_c \approx 2.05$.

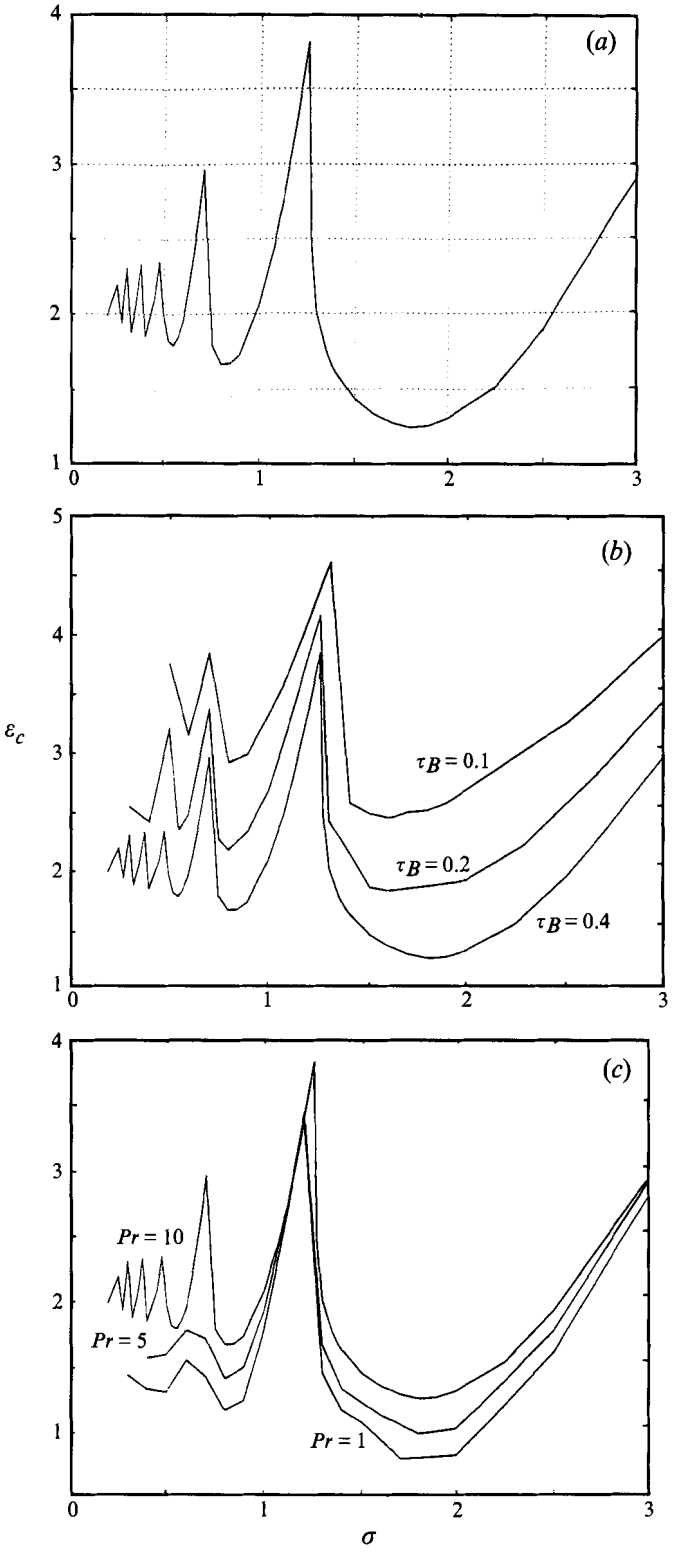

FIGURE 9. The effect on the stability limit of (*a*) frequency (*b*) τ_B and (*c*) Pr.

τ_B	Gr	μ_1	μ_2	μ_3
0.1	8×10^3	$1.898-0.00032i$	$-0.9366-0.000544i$	1.654
0.2	9×10^3	$1.084\times0.00030i$	$-0.3053-0.000027i$	1.214
0.3	1×10^4	$0.806-0.00028i$	$-0.1687-0.000080i$	1.119

TABLE 6. The variation of the coefficients μ_1, μ_2, and μ_3 as τ_B is varied. The other parameters are fixed at the same values as table 1: $Pr = 10$, $k = 0$. Gr is determined at each value of τ_B so that the damping of the eigenmode is 2×10^{-3}, the same as in table (4).

We have examined in some detail the effect of the parameters Ω and ϵ in destabilizing the eigenmodes corresponding to the steady problem, and have calculated the critical values of ϵ for which the instability is triggered. There are two other parameters in the governing equations: the stratification τ_B and the Prandtl number, which we will look into briefly now. Decreasing the stratification seems to have the effect of raising the stability limits, by increasing the value of ϵ_c, as shown in figure 9(*b*). The value of Gr for each τ_B was fixed so that the damping (given by the real part of $i\lambda$) of the modes was equal to 2×10^{-3}, the same as that for the initial case given in table 4. In table 6 we list the parameters and also the calculated coefficients μ_1, μ_2 and μ_3. Increasing the Prandtl number also has the same stabilizing effect, figure 9(*c*). This appears to be consistent with the observation in §2.3 that internal wave activity becomes weaker as the stratification is decreased or the Prandtl is increased, with the wave modes disappearing altogether at extreme values of these parameters. Thus it seems plausible that the modulation amplitude necessary to destabilize these modes would also increase with both τ_B and Pr.

This suggests that by pushing the parameters τ_B and Pr to extreme values, $Pr \gg 1$, $\tau_B \ll 1$, it might be possible to alter the behaviour that has been observed thus far. For this we consider two cases: one with high Prandtl number $Pr = 1000$, $\gamma = 1$, $Gr = 251$, $k = 0$; and a second case with small stratification and $Pr \sim O(1)$: $Pr = 0.73$; $Gr = 8.07\times10^3$, $\gamma = 1$, $k = 0$. In figure 10 we show the eigenspectra corresponding to these two cases. As can be seen, all the eigenvalues lie on the horizontal axis, implying that $\mathrm{Im}(i\lambda) = 0$, and hence they are damped stationary modes. Thus it appears that in the limit of large Pr and small τ_B the only modes that remain are stationary modes. Thus there is a curve, $\gamma_s(Pr)$ which divides (Pr, γ) into two regions, with the regions below the curve having only stationary modes. To explore this curve further we consider table 7 in which we show the values of γ_s as a function of Pr for fixed $Gr = 700.9\times10^3$. We note that for $\gamma < \gamma_s$ there are no travelling modes present. Further, in the last column we have displayed the stratification τ_{B_s} corresponding to γ_s. Surprisingly, τ_{B_s} has a nearly constant value of order 4×10^{-4}. This is independent of the choice of Grashof number. Thus from the definition of γ, we have the following simple expression for the γ_s curve in the (Pr, γ)-plane:

$$\frac{\gamma^4}{Gr\,Pr} \approx 10^{-4}. \tag{42}$$

Turning to the stability of the stationary modes when subjected to modulation, we find the following surprising result: the stationary modes when subjected to Floquet analysis (via equation (30)) were found to be stable to modulation amplitudes as large as $\epsilon = 30$.

Thus we find that for $\gamma < \gamma_s$, only the stationary modes survive in the long-wave limit, and these fail to interact with the modulation. We thus conclude that only the travelling modes of the system can interact with the modulation to produce instability.

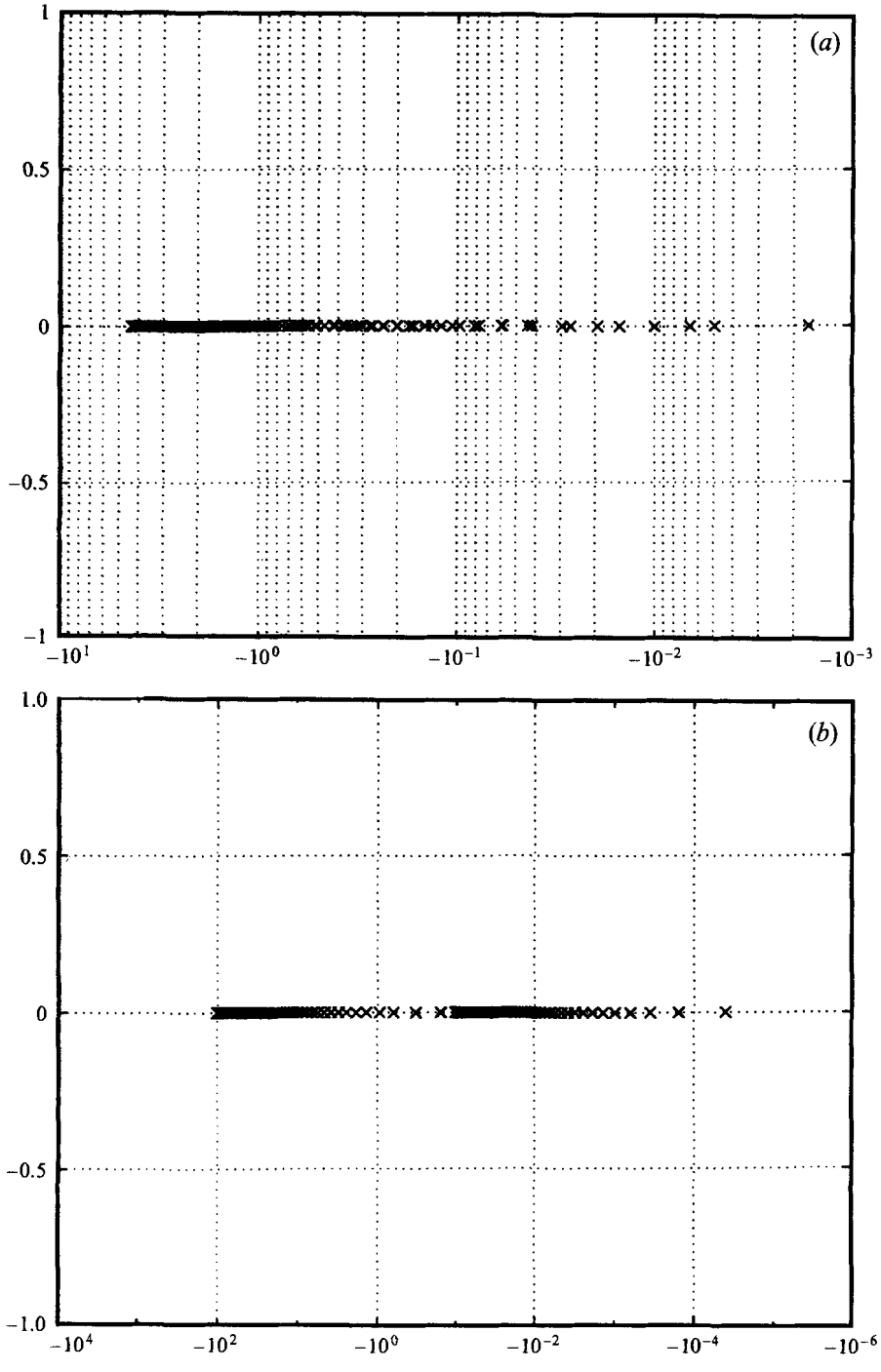

FIGURE 10. Eigenvalue spectrum for the case (*a*) $\gamma = 1$, $Pr = 0.73$, $Gr = 8.079 \times 10^3$ and $k = 0$, and (*b*) $\gamma = 1$, $Pr = 1000$, $Gr = 0.251 \times 10^3$ and $k = 0$, both showing the absence of any travelling modes.

Pr	γ_s	τ_{B_s}
0.73	2.0	1.258×10^{-4}
5.00	4.3	3.902×10^{-4}
10.00	5.0	3.560×10^{-4}
100.00	9.8	5.260×10^{-4}
1000.0	17.0	4.760×10^{-4}

TABLE 7. The dependence of γ_s on Pr for $Gr = 700.9 \times 10^3$. Also shown is the stratification, τ_{B_s}.

In the next subsection we consider the validity of these one-mode expansions by comparing them to the parallel-flow solutions of the full parallel-flow equations. There we will also consider some cases where $\gamma < \gamma_s$ and validate the present results.

4.4. *Parallel-flow solution of the full equations*

So far we have examined the behaviour of the slot problem subjected to gravity modulation by a severely truncated Galerkin expansion. By reducing the problem to a Mathieu equation we were able to show that under suitable conditions (of large amplitude of modulation) the system could be made unstable via parametric resonances of the Mathieu equation. It is possible that this behaviour is an artifact of the drastic truncation of the expansion (20). We will show here that this kind of behaviour is endemic to the parallel-flow solutions of (19) under gravity modulation.

The full time-dependent Boussinesq equations for parallel flow are

$$\left.\begin{aligned} Gr\,\Psi_{xxt} &= \Psi_{xxxx} - \Theta_x(1+\epsilon\cos\Omega t), \\ Ra\,\Theta_t - \tau_B\,Ra\,\Psi_x &= \Theta_{xx}. \end{aligned}\right\} \tag{43}$$

We note that (43) are linear, and parametrically forced. In some instances it has been possible to extend Floquet's theorem to partial differential equations[1], however (43) are not separable and hence such an extension has not been possible in the present case.

We interrogate (43) by full numerical simulation. For this purpose we consider case I of §2.3, whose eigenvalue spectrum we have shown in figure 5(*a*). The parameters for this case are $Gr = 7.009 \times 10^5$, $Pr = 0.73$, $\gamma = 12$. The long-wave eigenmode spectrum for this case (figure 5*a*) has a travelling mode with an eigenvalue $i\lambda = 0.6670 \times 10^{-4} \pm 0.487 \times 10^{-3}$i. The stability of this mode subjected to modulation has been examined via (35) and (41) and for $\Omega = 0.487 \times 10^{-3}$ the critical value of ϵ has been found to be 1.3.

We now proceed to verify the validity of this value by full simulation of (43). Equation (43) has been numerically integrated by (i) first semi-discretizing in space by standard second-order-accurate central differences and enforcing the boundary conditions and (ii) integrating the resulting system of ODEs in time by using a highly accurate (adaptive) solver. The forcing frequency has been chosen to be $\Omega = 0.487 \times 10^{-3}$, which corresponds to the natural frequency of the least-damped travelling mode in the spectrum as shown in figure 5(*a*). The results are summarized in table 5(*b*), where again (S) denotes stable solutions and (U) unstable ones. As can be seen the

[1] In solid-state physics for example, the motion of an electron in a crystal lattice is governed by the Schrödinger equation with a spatially periodic potential. Bloch (1928) showed that the Schrödinger equation under these circumstances admits normal solutions (called Bloch waves) which determine the stability of the electron motion, namely whether it will remain within the crystal or gain sufficient energy to be able to leave.

solution becomes unstable for $\epsilon = 0.8$. We recall that a value of 1.3 was obtained by applying Floquet theory to the one-mode expansion earlier. We thus conclude that the one-mode expansions of the governing equations considered so far succeeded in predicting the qualitative dynamics of the full set of equations subjected to gravity modulation.

Lastly we consider two cases where no travelling wave modes exist. First, consider a case with high $Pr = 1000$; the other parameters are $\gamma = 1$, $Gr = 251$, $\Omega = 5 \times 10^{-4}$. We found no evidence of any instability by carrying out full integrations of equation (43) for ϵ as high as 100. Then we considered a case with low stratification: $Pr = 0.73$, $Gr = 8070$, $\gamma = 1$, $\Omega = 5 \times 10^{-3}$ and again found no instability for ϵ as high as 500, confirming the results of the previous subsection.

5. Two-mode model of the slot

We have seen how parallel-flow solutions of the slot become unstable to gravity modulation. This was first seen from the stability analysis of modal evolution equations and by full numerical solution of the parallel-flow equations in the last section. This inevitably raises the question of how these parametric resonances have their growth limited.

The simplest reason for the unrestricted growth of the parallel solutions in the presence of modulation is that the parallel-flow equations have no nonlinear saturation mechanisms available to restrict growth. We recall that our studies for small ϵ showed that only the parallel-flow modes would be relevant. It therefore appears that for $\epsilon \sim O(1)$, this assumption is no longer true and it is necessary to bring in eigenmodes of finite axial wavenumber.

We therefore augment the original modal expansion scheme to include terms of finite axial wavenumber k as follows:

$$\left.\begin{aligned} \Psi &= \Psi_0(x) + B(t)\,\Psi_1(x) + D(t)\,\Psi_2(x)\,e^{iky} + \ldots + \text{c.c.}, \\ \Theta &= \Theta_0(x) + \tau_B y + A(t)\,\Theta_1(x) + C(t)\,\Theta_2(x)\,e^{iky} + \ldots + \text{c.c.}, \end{aligned}\right\} \tag{44}$$

where c.c. denotes the complex conjugate. Substituting the above expansion into the full equations (2) we find terms of the following three types: proportional to e^{iky}, e^{i0y} or parallel-flow terms independent of y, and e^{i2ky}. Thus collecting terms independent of y we have respectively for the vorticity transport and the energy equation

$$\begin{aligned} &Gr[B_t\,\Psi_1'' + B_t^*\,\Psi_1^{*''}] + ikDD^*Gr[\psi_2(\Psi_2^{*'''} - k^2\Psi_2^{*'}) - \psi_2^*(\Psi_2''' - k^2\Psi_2') \\ &\quad + \psi_2'(\Psi_2^{*''} - k^2\Psi_2^*) - \psi_2^{*'}(\Psi_2'' - k^2\Psi_2)] \\ &\qquad = B\Psi_1^{iv} + B^*\Psi_1^{*iv} - [A\Theta_1' + A^*\Theta_1^{*'}](1 + \epsilon\cos\Omega t), \end{aligned} \tag{45}$$

$$\begin{aligned} &Ra[A_t\,\Theta_1 + A_t^*\,\Theta_1^*] + ik\,Ra[DC^*(\Psi_2\,\Theta_2^{*'} + \Psi_2'\Theta_2^*) - D^*C(\Psi_2^*\,\Theta_2' + \Psi_2^{*'}\,\Theta_2)] \\ &\qquad - \tau_B\,Ra\,B\Psi' + \tau_B\,Ra\,B^*\Psi^{*'} = A\Theta_1'' + A^*\Theta_1^{*''}. \end{aligned} \tag{46}$$

Similarly collecting terms proportional to e^{iky}, we get the following two equations:

$$\begin{aligned} &Gr\,D_t(\Psi_2'' - k^2\Psi_2) + (ikGr\,D[\Psi_2\,\Psi_0''' - (\Psi_2'' - k^2\Psi_2)\,\Psi_0'] \\ &\quad + ikGr\,DB[\Psi_2\,\Psi_1''' - (\Psi_2'' - k^2\Psi_2)\,\Psi_1'] + ikGr\,DB^*[\Psi_2\,\Psi_1^{*'''} - (\Psi_2'' - k^2\Psi_2)\,\Psi_1^{*'}] \\ &\qquad = D[\Psi_2^{iv} - 2k^2\Psi_2'' + k^4\Psi_2] - C\Theta_2'(1 + \epsilon\cos\Omega t), \end{aligned} \tag{47}$$

$$\begin{aligned} &Ra\,C_t\,\Theta_2 + D[ik\,Ra\,\Psi_2\,\Theta_0' - \tau_B\,Ra\,\Psi_2'] + ADik\,Ra\,\Psi_2\,\Theta_1' + A^*Dik\,Ra\,\Psi_2\,\Theta_1^{*'} \\ &\quad - CBik\,Ra\,\Theta_2\,\Psi_1' - CB^*ik\,Ra\,\Theta_2\,\Psi_1^{*'} - C[ik\,Ra\,\Theta_2\,\Psi_0' + (\Theta_2'' - k^2\Theta_2)] = 0. \end{aligned} \tag{48}$$

We now form Galerkin dot products in the usual way, giving the following dynamical system of equations for the time-dependent Fourier coefficients:

$$\nu_{11} B_t + \nu_{12} B_t^* + \nu_{13} DD^* = \nu_{14} B + \nu_{15} B^* + \epsilon\nu_{16} \cos \Omega t + (\nu_{17} A + \nu_{18} A^*)(1 + \epsilon \cos \Omega t), \tag{49}$$

$$\nu_{31} A_t + \nu_{32} A_t^* + \nu_{33} DC^* + \nu_{34} D^* C + \nu_{35} B + \nu_{36} B^* = \nu_{32} A + \nu_{38} A^*, \tag{50}$$

$$\nu_{21} D_t + \nu_{22} D + \nu_{23} DB + \nu_{24} DB^* = \nu_{25}(1 + \epsilon \cos \Omega t) C, \tag{51}$$

$$\nu_{41} C_t + \nu_{42} D + \nu_{43} AD + \nu_{44} A^* D + \nu_{45} CB + \nu_{46} CB^* + \nu_{47} C = 0. \tag{52}$$

The definitions for the coefficients in (49)–(52) are given in Appendix B. Equations (49)–(52), rescaled as

$$A_\epsilon = \epsilon A, \quad B_\epsilon = \epsilon B, \quad C_\epsilon = \epsilon C, \quad D_\epsilon = \epsilon D, \tag{53}$$

assume the form

$$\nu_{11} B_{\epsilon t} + \nu_{12} B_{\epsilon t}^* + \underline{\epsilon\nu_{13} D_\epsilon D_\epsilon^*} = \nu_{14} B_\epsilon + \nu_{15} B_\epsilon^* + \nu_{16} \cos \Omega t + (\nu_{17} A_\epsilon + \nu_{18} A_\epsilon^*)(1 + \epsilon \cos \Omega t), \tag{54}$$

$$\nu_{31} A_{\epsilon t} + \nu_{32} A_{\epsilon t}^* + \underline{\epsilon\nu_{33} D_\epsilon C_\epsilon^*} + \underline{\epsilon\nu_{34} D_\epsilon^* C_\epsilon} + \nu_{35} B_\epsilon + \nu_{36} B_\epsilon^* = \nu_{37} A_\epsilon + \nu_{38} A_\epsilon^*, \tag{55}$$

$$\nu_{21} D_{\epsilon t} + \nu_{22} D_\epsilon + \underline{\epsilon\nu_{23} D_\epsilon B_\epsilon} + \underline{\epsilon\nu_{24} D_\epsilon B_\epsilon^*} = \nu_{25}(1 + \epsilon \cos \Omega t) C_\epsilon, \tag{56}$$

$$\nu_{41} C_{\epsilon t} + \nu_{42} D_\epsilon + \underline{\epsilon\nu_{43} A_\epsilon D_\epsilon} + \underline{\epsilon\nu_{44} A_\epsilon^* D_\epsilon} + \underline{\epsilon\nu_{45} C_\epsilon B_\epsilon} + \underline{\epsilon\nu_{46} C_\epsilon B_\epsilon^*} + \nu_{47} C_\epsilon = 0. \tag{57}$$

This system of four equations represents the evolution equations when two modes (and their complex conjugates) are used in expansion (44). We note that (54)–(57) are nonlinear and non-autonomous. Since A_ϵ, B_ϵ, C_ϵ, D_ϵ are each complex valued, (54)–(57) can each be separated into real and imaginary parts, thus yielding a dynamical system in nine-dimensional phase space.

The nonlinear terms in (54)–(57) have been underlined. The quadratic nonlinearities arise from the nonlinear convective terms in the energy and vorticity transport equations and represent coupling between the parallel-flow and finite-wavenumber modes, or between complex-conjugate parallel-flow modes. In the next subsection we will examine the method of solution of these equations.

5.1. *Numerical results*

To understand the behaviour of (54)–(57) we need to make a particular choice for the coefficients. Let us consider the case that was examined in §4.4, choosing $Pr = 0.73$, $Gr = 7.009 \times 10^5$, and $\gamma = 12$, for which we have found the least-damped parallel eigenmode to have an eigenvalue $i\lambda = 0.6670 \times 10^{-4} \pm 0.487 \times 10^{-3}i$. We also noted in §4.4 that this eigenmode becomes unstable when subjected to gravity modulation for $\epsilon > 1.3$ at its natural frequency. Henceforth we will refer to this mode as the primary mode.

If a second finite-wavenumber mode is to come into play in the dynamics, the natural choice for this mode would be the one that is least damped over all the wavenumbers. This is found to be a travelling mode at $k = 3.52$ with eigenvalue $i\lambda = 0.3252 \times 10^{-5} \pm 1.6903 \times 10^{-3}i$, which we will henceforth refer to as the secondary mode. With this choice of modes in (44) the coefficients in (54)–(57) can be evaluated with the aid of (B 1)–(B 4). Thus we can now investigate the behaviour of the dynamical system (54)–(57). It has been solved using a highly accurate adaptive solver for time integration. The accuracy of the solutions has been verified by mesh refinement. We will discuss these solutions in the coming subsections.

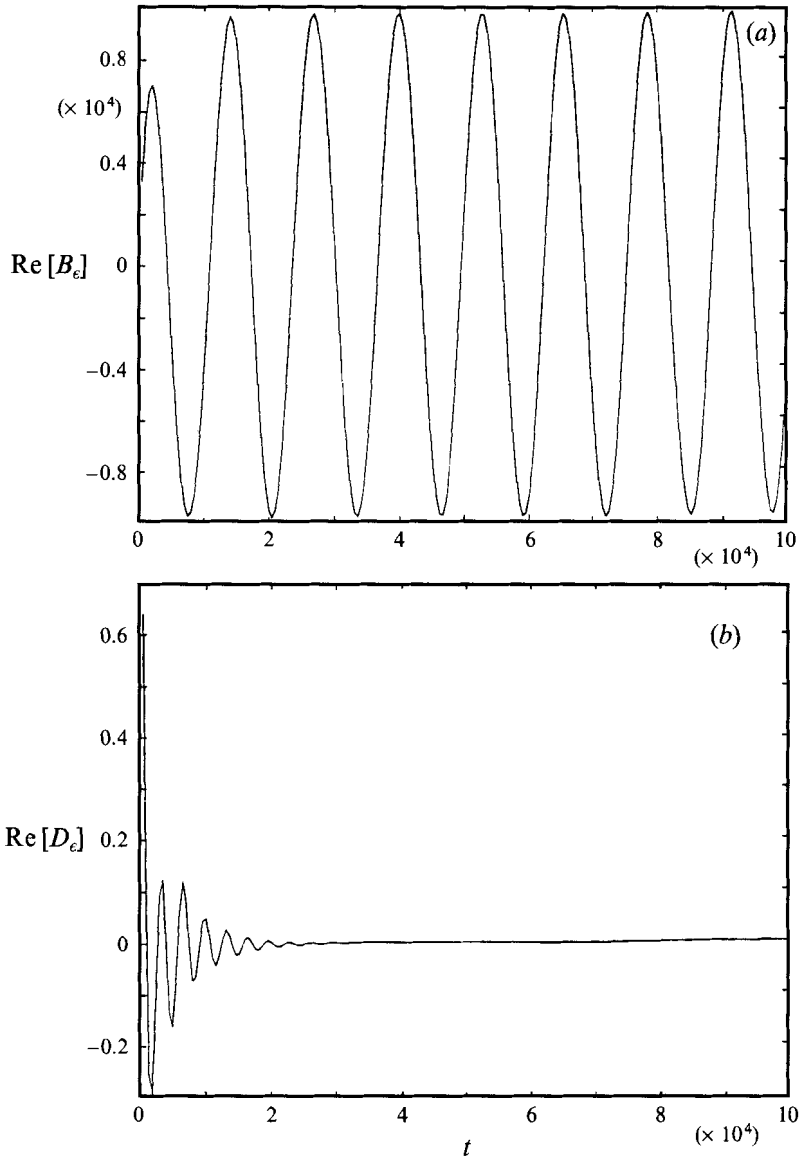

FIGURE 11. (*a*) Re[B_ϵ] showing linear forced response. (*b*) Re[D_ϵ] showing decaying oscillations. $\epsilon = 0.1$.

5.2. *Nonlinear stability of the unmodulated problem*

We begin by pointing out that the modes that we have picked are both linearly damped modes. This raises the question of whether, in the absence of modulation, the solutions to the initial value problem (54)–(57) decay to zero at $t < \infty$. The damping rate of the two modes is quite small (0.6670×10^{-4} and 0.3252×10^{-5} respectively) and they are therefore very near the bifurcation point. We can easily determine if this bifurcation is subcritical by taking (54)–(57) for the unmodulated slot problem obtained by setting $\cos \Omega t$ identically to zero, and solving them using a wide variety of finite-amplitude initial conditions. Following this procedure, as far as we could determine the bifurcation is not subcritical. Thus the dynamics of the unmodulated problem are given

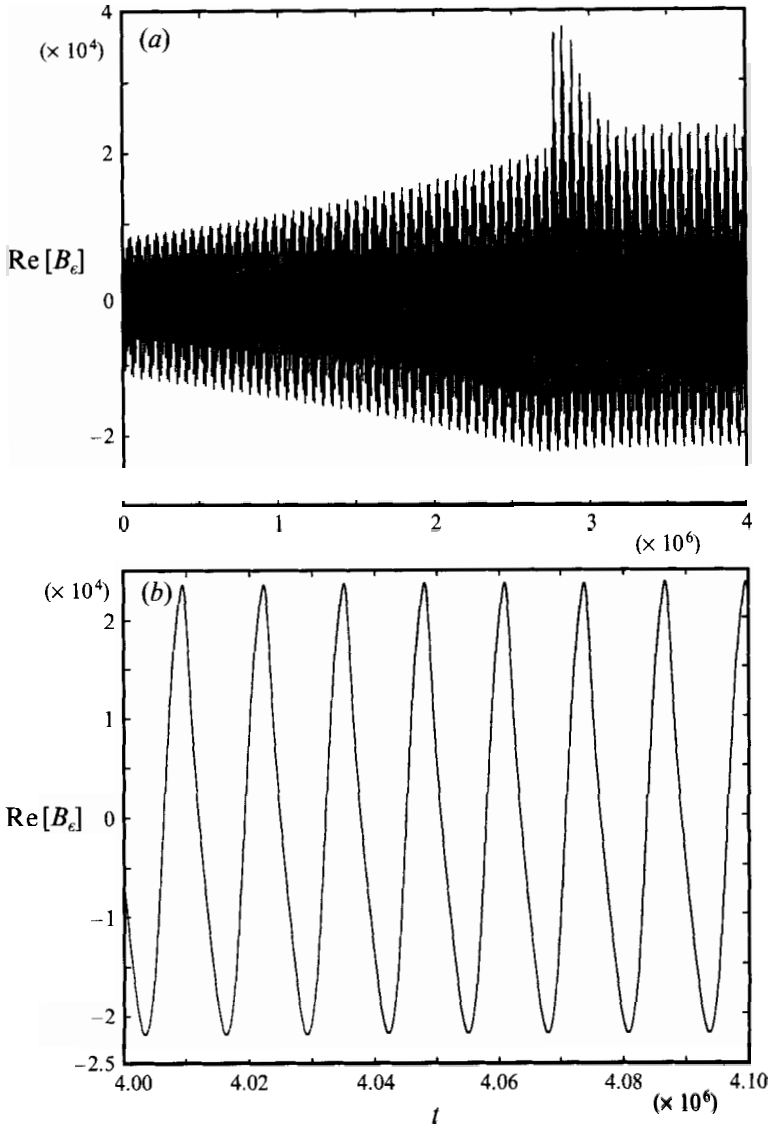

FIGURE 12. (*a*) Re[B_ϵ] for $\epsilon = 1.31$, showing growth and saturation. (*b*) As (*a*) but on a larger scale, showing saturation to a steady oscillation.

by the linearized form of equation (54)–(57) which predicts that both modes decay at $t \to \infty$.

5.3. *Small-ϵ modulation of the two-mode problem*

We now turn to the modulated problem, where we begin by taking small ϵ. Consider figure 11 where we show a sample of results for $\epsilon = 0.01$. Recall that we have eight dependent variables in the dynamical system (54)–(57). Here figure 11(*a*) shows the temporal evolution of Re[B_ϵ] and figure 11(*b*) shows Re[D_ϵ]. These plots are representative of the dynamics of the two modes, i.e. the primary mode oscillates and the secondary mode decays for small ϵ. We note that the oscillation of the primary mode is produced by the inhomogeneous forcing term in (54). There is no

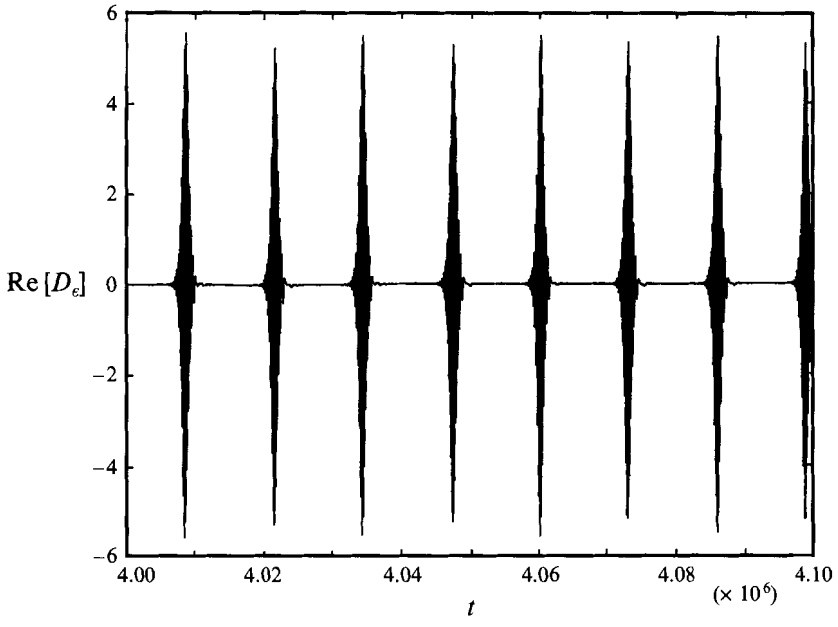

FIGURE 13. Re$[D_\epsilon]$ for $\epsilon = 1.31$, showing high-frequency bursting with recurrence synchronous with driving frequency.

inhomogeneous forcing term in (56) or (57) which accounts for the decay of the secondary mode. We have alluded to this earlier by saying that it is only the primary mode that is directly forced by the modulation. Thus we find that in the limit of small ϵ the secondary mode is not excited and the only activity is due to the forced oscillations of the primary mode.

This can be seen from (54)–(57) in the limit $\epsilon \to 0$. Thus upon linearizing, we are left with the following linear system:

$$\nu_{11} B_{\epsilon t} + \nu_{12} B^*_{\epsilon t} = \nu_{14} B_\epsilon + \nu_{15} B^*_\epsilon + \nu_{16} \cos \Omega t + (\nu_{17} A_\epsilon + \nu_{18} A^*_\epsilon)(1 + \epsilon \cos \Omega t), \quad (58)$$

$$\nu_{31} A_{\epsilon t} + \nu_{32} A^*_{\epsilon t} = -\nu_{35} B_\epsilon - \nu_{36} B^*_\epsilon + \nu_{37} A_\epsilon + \nu_{38} A^*_\epsilon, \quad (59)$$

$$\nu_{21} D_{\epsilon t} = -\nu_{22} D_\epsilon + \nu_{25}(1 + \epsilon \cos \Omega t) C_\epsilon, \quad (60)$$

$$\nu_{41} C_{\epsilon t} = -\nu_{42} D_\epsilon - \nu_{47} C_\epsilon = 0. \quad (61)$$

These represent two decoupled, parametrically forced, linear systems the stability of which can be examined by Floquet theory. We have already mentioned that the primary mode is stable for $\epsilon < 1.3$ and is thus stable in the limit of small ϵ which we are at present considering. The second system has been found to have a critical $\epsilon_{c2} = 2.9$, and thus it is also stable in the limit of small ϵ.

5.4. *Effect of ϵ on two-mode dynamics*

What happens when ϵ is increased? We have numerically verified that the behaviour seen for small ϵ holds so long as $\epsilon < \epsilon_{c1}$. For $\epsilon > \epsilon_{c1}$, the primary mode becomes unstable and grows in accord with Floquet theory. In the absence of any nonlinear saturation mechanisms this growth would continue unchecked making the solutions unbounded at $t \to \infty$. The effect of the nonlinear terms, as we shall presently see, is to limit the amplitude of the growing mode thus keeping the solution bounded. In figure 12(*a*) we plot the evolution of Re$[B_\epsilon]$ over time for $\epsilon = 1.31$ which is only slightly

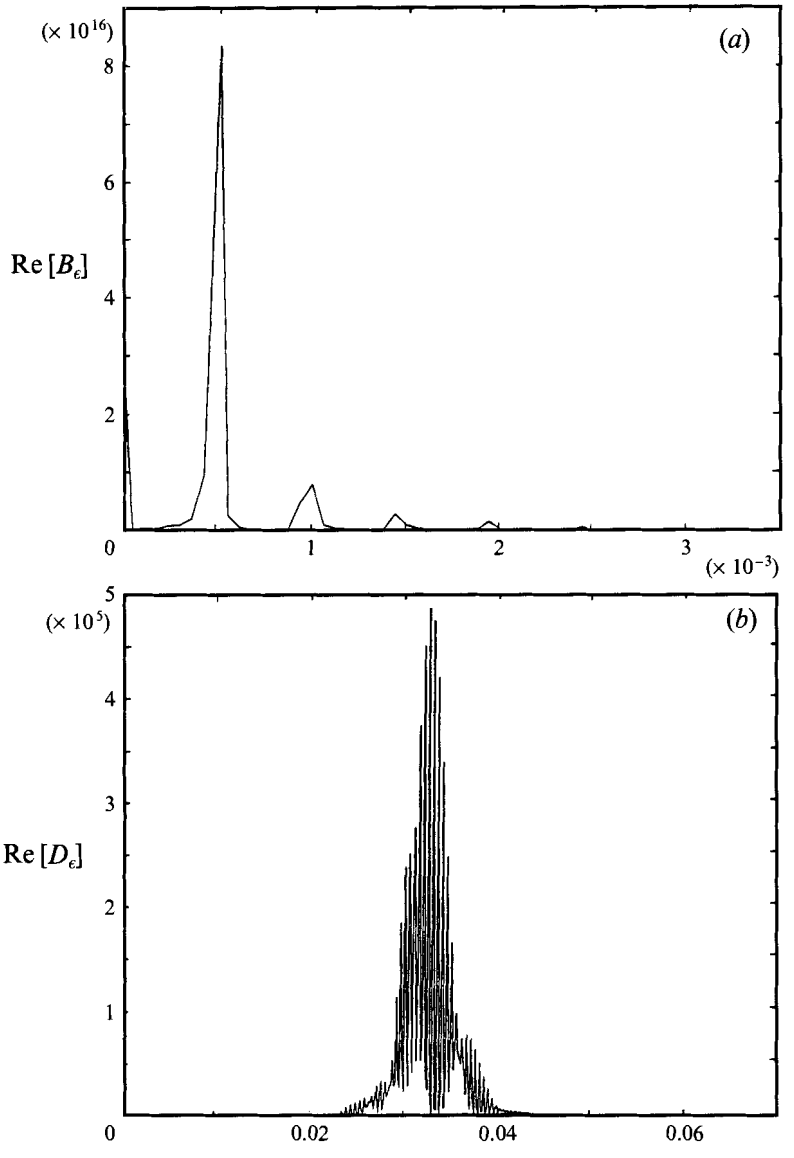

FIGURE 14. (*a*) The energy spectrum $E_{\mathrm{Re}[B_\epsilon]}$ for $\epsilon = 1.31$. Note the peaks at the fundamental forcing frequency and the higher harmonics. (*b*) Energy spectrum $E_{\mathrm{Re}D_\epsilon}$ for $\epsilon = 1.31$ showing broad-band high-frequency content of bursts.

higher than $\epsilon_{c1} = 1.30$. We note that the solution shows transient growth, but for $t > 4.0 \times 10^6$ it equilibrates and the amplitude reaches its steady value. This behaviour is also seen for $\mathrm{Im}[B_\epsilon]$ and the real and imaginary parts of A_ϵ which have thus not been shown. In figure 12(*b*) we show the steady-state oscillations of $\mathrm{Re}[B_\epsilon]$ (on a larger scale), which are periodic with period $T = 2\pi/\Omega = 12901.8$. Thus the oscillations are synchronous with the driving frequency. The steady-state behaviour of $\mathrm{Re}[D_\epsilon]$ is shown in figure 13, and is seen to consist of periodic bursts, which again occur with period $T = 12901.8$; thus there is one burst for each cycle of the driving frequency. This behaviour is also seen with $\mathrm{Im}[D_\epsilon]$ and C_ϵ (not shown). We now begin to see the mechanism by which the primary mode is saturated: the primary mode becomes

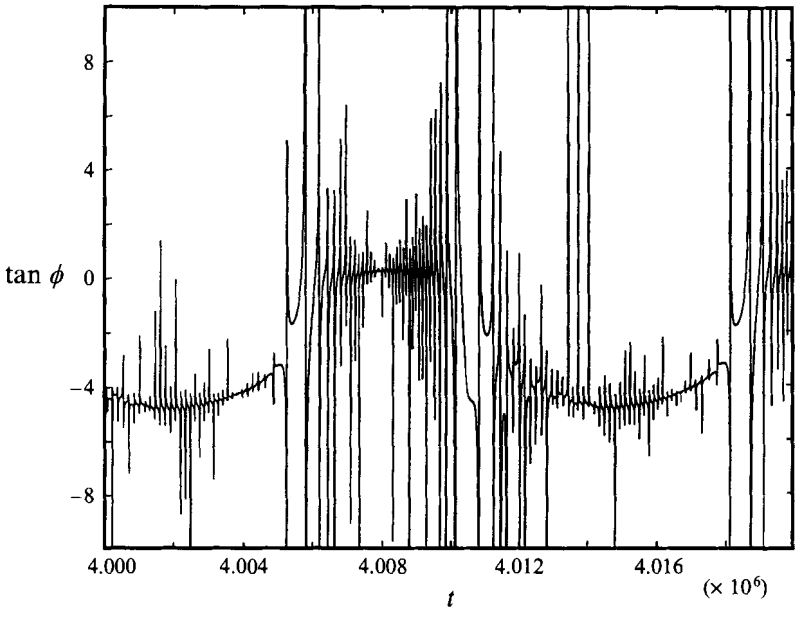

FIGURE 15. Phase, $\tan\phi$, of nonlinear term $D_\epsilon C_\epsilon^*$ for $\epsilon = 1.31$.

unstable and starts to grow. The secondary mode, which is linearly damped, only gets excited when the amplitude of the primary mode is large enough to overcome the damping. The excess of energy which the primary mode gains from the gravity modulation over each period of the driving frequency (which is potentially capable of producing growth) is now pumped into the secondary mode, and used in overcoming the damping present in that mode. Thus there is a periodic burst in the secondary mode which consumes just enough energy to prevent unstable growth of the primary mode. This kind of bursting behaviour has also been seen by Aubry *et al.* (1988) who have modelled the wall region of a turbulent boundary layer by expanding the Navier–Stokes equations using experimentally determined streamwise rolls as the basis functions. The resulting dynamical system showed intermittency or bursts and they have tried to relate this to ejection and bursting events observed by Kline *et al.* (1967) in a turbulent boundary layer.

In figure 14 we show the energy spectra of $\mathrm{Re}[B_\epsilon]$ and $\mathrm{Re}[D_\epsilon]$, $E_{\mathrm{Re}[B_\epsilon]}$ and $E_{\mathrm{Re}[D_\epsilon]}$ respectively. As can be seen (in figure 14*a*) the energy for $\mathrm{Re}[B_\epsilon]$ shows a peak at 4.7×10^{-4} which corresponds to the driving frequency, and several smaller peaks at the superharmonics of the driving frequency. Figure 14(*b*) shows that $\mathrm{Re}[D_\epsilon]$ has a broad-banded energy spectrum, with a broad peak at a frequency of ≈ 0.033 which is much higher than the driving frequency of 0.487×10^{-3}.

This kind of intermittency in dynamical systems theory is often associated with the existence of two states: a quiescent laminar state in which the solution trajectory spends most of the time, and a second unstable state, with high-frequency bursts being the result of state switching. In order to explore the mechanics of these bursting phenomena further, we interrogate the nonlinear terms in the dynamical system (54)–(57). Consider (55), which has the nonlinear terms $D_\epsilon C_\epsilon^*$ and $D_\epsilon^* C_\epsilon$. Since D_ϵ and C_ϵ^* are each complex valued, $D_\epsilon C_\epsilon^*$ is also complex valued. In figure 15 we show the phase (or the complex argument, $\tan\phi = \mathrm{Re}[D_\epsilon C_\epsilon^*]/\mathrm{Im}[D_\epsilon C_\epsilon^*]$) of the nonlinear term $D_\epsilon C_\epsilon^*$ as a function of time for $\epsilon = 1.31$. The scale of the y-axis has been arbitrarily

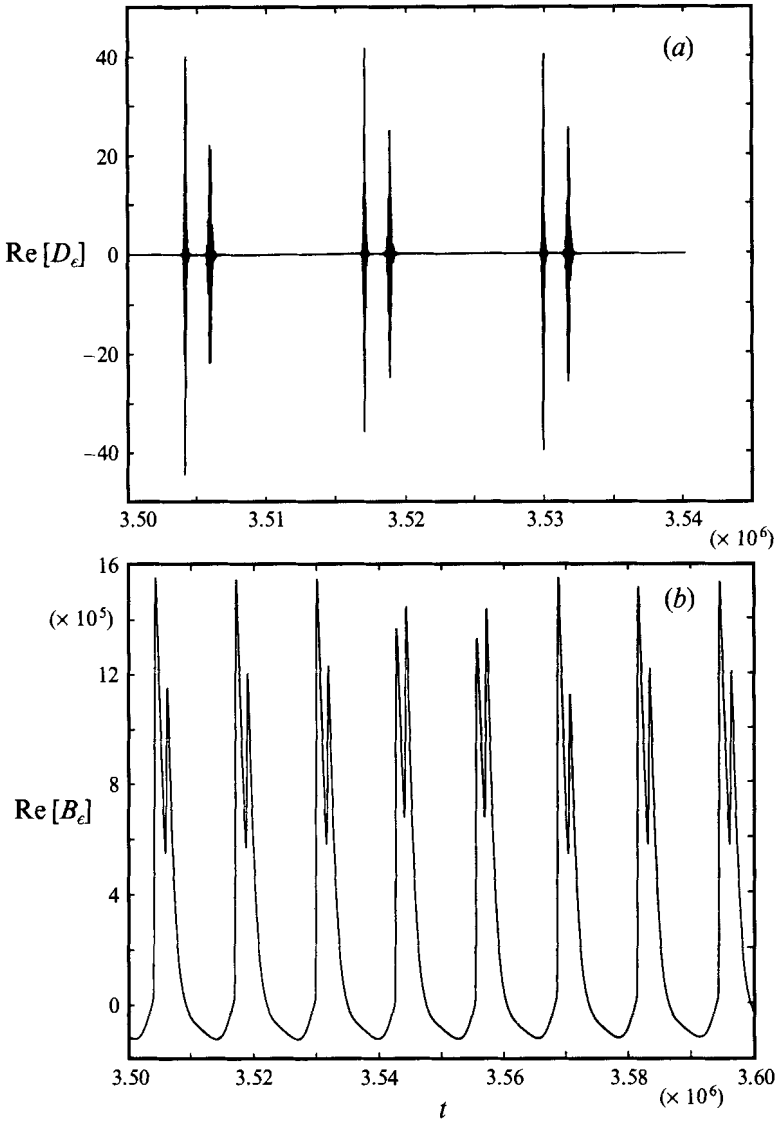

FIGURE 16. (*a*) Re[D_ϵ] at $\epsilon = 1.43$. Note that the response consists of two peaks. (*b*) Re[B_ϵ] at $\epsilon = 1.43$ showing the 'spike'.

limited to the interval $(-10, 10)$, and we therefore treat the boundary values of the interval, ± 10, as numerical 'infinity' for the tangent function, $\tan\phi$. It is evident from the plot that the phase shows very high-frequency oscillations. However, despite the high-frequency noise, two states are distinguishable: a state where the phase $\tan\phi \approx -4$, and another state when $\tan\phi$ is positive, but only slightly greater than zero. Thus there is an almost $\frac{1}{2}\pi$ phase jump between these two states, which is accompanied by very high-frequency oscillations. It is possible to identify the first state with the quiescent laminar region of the secondary mode (compare with figure 13) and the second state with the turbulent burst of the secondary mode, because they coincide in time. Thus the following picture emerges: the secondary mode spends most of the time in the first state, where the nonlinear term has a negative sign and thus limits its growth.

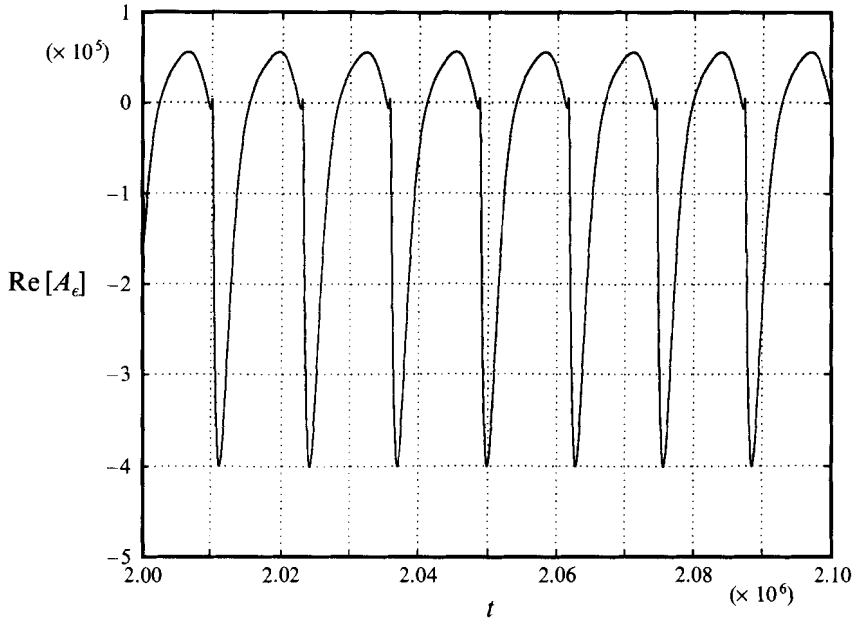

FIGURE 17. $\mathrm{Re}[A_\epsilon]$ at $\epsilon = 1.40$ showing the onset of the tertiary instability.

This corresponds to the quiescent region of the secondary mode; however, there is a second state which is unstable and switching between these states is accompanied by high-frequency oscillations.

As ϵ is increased, the initial growth of the primary mode becomes more rapid, making the saturation process even more nonlinear. It eventually reaches a steady state as before, but the response of the secondary mode shows a curious splitting, seen in figure 16(*a*), which shows $\mathrm{Re}[D_\epsilon]$ for $\epsilon = 1.43$. In figure 16(*b*) we show the steady response of $\mathrm{Re}[B_\epsilon]$ also at $\epsilon = 1.43$ where a 'spike' has developed in the periodic oscillations. The onset of this tertiary instability seems to occur at $\epsilon \approx 1.4$ (shown in figure 17), and the secondary burst becomes stronger as ϵ is increased further (as shown previously in figure 16*a*)). Figure 18 shows the energy spectrum, E_{B_ϵ}, E_{D_ϵ} for $\epsilon = 1.43$. E_{B_ϵ} has many higher harmonics at 2, 3, 4, 5, 6, 7, 8, 9 times the fundamental frequency. E_{D_ϵ} shows a very broad peak with energy at very high frequencies. In figure 19 we show the phase of the term $D_\epsilon C_\epsilon^*$ for $\epsilon = 1.43$. Again we see two states as before; however the second state appears to be more distinct, with less noise from high-frequency oscillations, indicating that the trajectory does indeed spend some time in this state. Since the phase of the nonlinear term differs in the second state by $\frac{1}{2}\pi$, this weakens the nonlinear saturation mechanism, which might help explain the tertiary instability or spike that has been observed.

5.5. *Effect of varying the parameters*

The two-mode problem is governed by five parameters: τ_B, Pr, Gr, k and Ω. The effect of τ_B, Pr, Gr and k on equations (54)–(57) is felt through the coefficients computed via (74)–(101).

In the previous subsection we have seen that the value of ϵ_{c1}, the critical modulation amplitude for the primary mode, plays a critical role in determining the overall dynamics of the problem. A detailed parametric study of the behaviour of ϵ_{c1} has already been carried out in §4.3 and we recall this in connection with the present two-

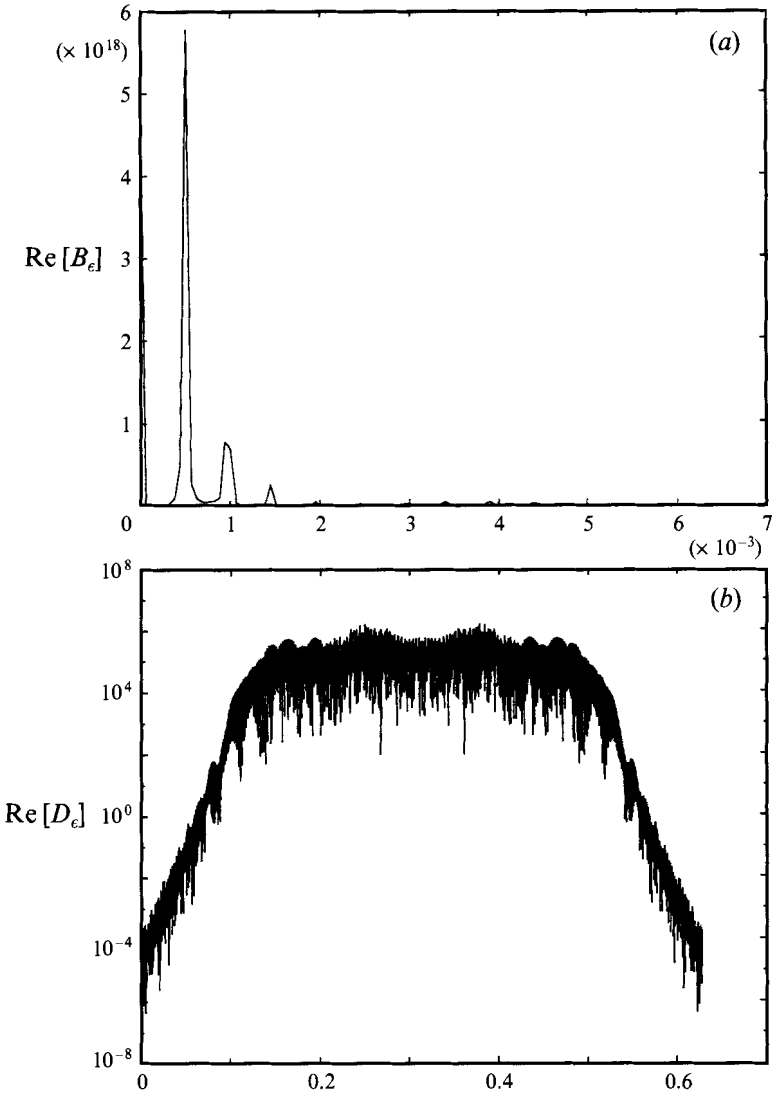

FIGURE 18. (*a*) Energy spectrum, $E_{\mathrm{Re}[B_\epsilon]}$ for $\epsilon = 1.43$, showing higher harmonics. (*b*) Energy spectrum, $E_{\mathrm{Re}D_\epsilon}$ for $\epsilon = 1.43$, showing broad-band high-frequency content of bursts.

mode problem: increasing the stratification is destabilizing whereas decreasing Pr has the same effect. The influence of frequency of ϵ_{c1} is complicated, but higher frequencies raise the threshold, ϵ_{c1}. At lower frequencies, the value of ϵ_{c1} shows many bounded maxima and minima, approaching the value 2.05 in the limit of quasi-static modulation.

Further we noted in §4.3 that in the limit of large Pr and small stratification, it was no longer possible to excite the parametric instability of the primary mode. This has an immediate effect on the results of the two-mode model of this section as well. If the primary mode shows no parametric instability, then the secondary mode simply damps out and decays.

There are other parameters to consider. Noting that varying the frequency can alter the value of ϵ_{c1}, we now turn to an interesting question. In the previous subsection, we studied a case where the threshold of modulation-induced instability was lower for the

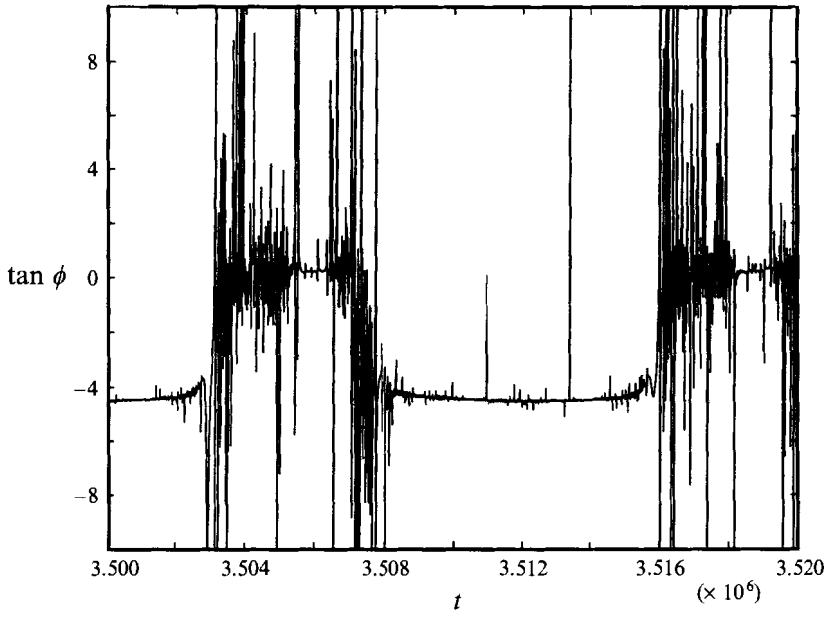

FIGURE 19. Nonlinear term $D_t C_\epsilon^*$ for $\epsilon = 1.43$.

primary mode than the secondary, i.e. $\epsilon_{c1} < \epsilon_{c2}$. We now ask what would happen if $\epsilon_{c2} < \epsilon_{c1}$ implying that the secondary mode has a lower threshold of modulation-induced stability than the primary.

This situation can be realized by considering the case of the previous subsection at a forcing frequency given by $\Omega = 1.7 \times 10^{-3}$. The values of $\epsilon_{c1,2}$ for this value of Ω have been estimated to be $\epsilon_{c1} = 4.5$ and $\epsilon_{c2} = 3.6$ as computed by (58)–(61). Thus according to the linearized equations (58)–(61), $\epsilon_{c2} < \epsilon_{c1}$.

We expect therefore, that for $\epsilon_{c2} < \epsilon < \epsilon_{c1}$ the secondary mode would start to grow first, until the nonlinear saturation becomes strong enough to take effect. However, this scenario is not born out by the solution of the full nonlinear equations (54)–(57). For $\epsilon_{c2} < \epsilon < \epsilon_{c1}$, the secondary mode simply decays. Only when $\epsilon > \epsilon_{c1}$ and the primary mode starts to grow does the secondary mode get engaged as we have seen in the previous subsection.

The reason for this behaviour is not hard to find. The primary mode is driven by the inhomogeneous term in (54) and thus has a non-zero, oscillating solution. Thus it is not accurate to ignore it (as we have) in (54)–(57) except when ϵ is small. Since we are using $\epsilon \sim O(1)$, the results of the linearized equation for the secondary mode are likely to yield inaccurate results as we have verified.

However it is conceivable that there might be other parameter regimes where the secondary mode might indeed become unstable first. We have not found any case where this happens, and this reinforces the assumption we made earlier that in the context of the slot problem it is the parallel-flow modes that dominate the dynamics of the flow.

6. Summary and conclusions

In this paper we have investigated a slot problem subjected to gravity modulation. We began by studying the linear stability of the laminar base flow in the case of a steady gravitational field, and found three types of modes: travelling boundary-layer modes,

stationary modes and internal wave modes associated with the stratification in the slot. We noted that the internal wave modes are the only oscillatory modes to survive in the long-wave $k = 0$ limit, and these disappear too when the Prandtl number is very high or the stratification is low.

To examine the effect of gravity modulation, we first assumed small-amplitude modulation by considering regular perturbation expansions of the equations in ϵ and showed the existence of resonances when the modulation frequency matches the frequency of the natural modes of the system. Next we examined the stability of the long-wave eigenmodes of the slot problem when subjected to gravity modulation of $O(1)$ magnitude. This was achieved by projecting the governing equations onto the least-damped eigenmode, and recasting the resulting dynamical equation into the form of a Mathieu equation which was then investigated via Floquet theory. The chief conclusion is that the parallel-flow modes can be made unstable when subjected to modulation of suitable amplitude. We have examined the effect of the forcing frequency on ϵ_c, the critical modulation amplitude that triggers the instability, and the results show that ϵ_c is generally high for large frequencies, but for small frequencies the behaviour is complex. At very low frequencies, the equation becomes very stiff and we have therefore used WKB theory to find the stability limit for quasi-static modulation. We verified that the one-mode expansion of the parallel equations for the slot problem gave an accurate representation of the relevant dynamics of the problem by comparing with the results of full simulation of the parallel-flow equations for the slot. The critical value of the modulation amplitude, ϵ_c, for instability in the two cases was 1.3 and 0.8 respectively. Thus they show qualitative agreement. To consider the effect of varying the parameters we looked at the effect of stratification on the stability and found that when stratification is small, or Pr is large, the internal wave presence is weak, and hence the IW modes are more stable to gravity modulation. Finally we noted that in the limit of extremely high Pr or low stratification, the flow cannot be destabilized by the modulation.

We noted that the parallel-flow equations have no nonlinear saturation mechanisms, which allows the solution to grow without bound. To overcome this difficulty we undertook a two-mode expansion of the problem with the primary mode being the least-damped parallel-flow mode as before and a secondary mode of finite wavenumber. By projecting the governing equations onto these two modes we obtained the equations for temporal evolution of the two modes. A detailed numerical solution of these evolution equations showed that so long as the value of ϵ was kept below the critical value for the instability of the primary mode, the primary mode oscillated synchronously with the forcing and the secondary mode decayed. But when this critical value of ϵ was exceeded, the primary mode started to grow until the growth was saturated by nonlinear coupling with the secondary mode. As a result of this coupling the secondary mode is excited and shows intermittent 'bursts', which appeared once every cycle of the forcing frequency. Thus excess energy from the primary mode is used to excite and sustain the (otherwise damped) oscillations of the secondary mode.

The authors acknowledge the support of NASA, Grant NAG-3-1475.

Appendix A. The effect of quasi-static modulation: $\sigma \to 0$

We start with equation (36),

$$\eta_{\tau\tau} + \frac{1}{\sigma^2} Q(\tau)\, \eta = 0,$$

and wish to find its solution in the limit $\sigma \to 0$. In accordance with the standard WKB technique we seek solutions for the form

$$\eta = \exp\left(\frac{1}{\sigma} G\left(\tau, \frac{1}{\sigma}\right)\right), \tag{A 1}$$

where G has a straightforward expansion in terms of σ. Differentiating (A 1) twice yields

$$\eta' = \frac{1}{\sigma} G' \exp\left(\frac{1}{\sigma} G\right), \quad \eta'' = \left(\frac{1}{\sigma^2} G'^2 + \frac{1}{\sigma} G''\right) \exp\left(\frac{1}{\sigma} G\right).$$

Substituting for η, η', η'' in the linear equation (36), we transform it into the following nonlinear equation:

$$\frac{1}{\sigma^2} G'^2 + \frac{1}{\sigma} G'' + \frac{1}{\sigma^2} Q = 0 \tag{A 2}$$

and

$$G'^2 + \sigma G'' + Q = 0. \tag{A 3}$$

We seek a straightforward expansion for G in the form

$$G(\tau; \sigma) = G_0(\tau) + \sigma G_1(\tau) + \ldots. \tag{A 4}$$

Equating the coefficients of σ^0 and σ to zero, we obtain

$$G_0'^2 + Q(\tau) = 0, \quad G_0'' + 2G_0' G_1' = 0. \tag{A 5), (A 6}$$

It follows from (A 5) that $G_0'^2 = -Q(\tau)$, so that

$$G_0' = \pm \mathrm{i} (Q(\tau))^{1/2}. \tag{A 7}$$

Then,

$$G_0 = \pm \int \mathrm{i} (Q(\tau))^{1/2} \, \mathrm{d}\tau. \tag{A 8}$$

To solve (A 6), we divide it first by $2G_0'$ and obtain

$$\frac{1}{2} \frac{G_0''}{G_0'} + G_1' = 0 \tag{A 9}$$

which, upon integration gives

$$G_1 = -\ln (G_0')^{1/2}. \tag{A 10}$$

Substituting for G_0 and G_1 in (A 4) and using (A 1) we get after some simplification:

$$\eta \approx \frac{\exp\left[\pm \frac{\mathrm{i}}{\sigma} \int Q^{1/2} \, \mathrm{d}\tau\right]}{\sqrt{\pm \mathrm{i}}\, Q^{1/4}}. \tag{A 11}$$

Equation (A 11) provides two linearly independent approximate solutions of (36) in the limit $\sigma \to 0$. Now the integrand in (A 11) is a complex-valued oscillating function. We want to find the imaginary part of its mean asymptotic slope, denoted as S. For stability (using (34)) we get the criterion

$$S = \mathrm{Im}\left[\lim_{\tau \to \infty} \frac{\mathrm{d}}{\mathrm{d}t} \int Q^{1/2} \, \mathrm{d}\tau\right] < \mathrm{Re}\left[\frac{\mu_1}{2}\right] \tag{A 12}$$

and $\bar{Q}$ denotes the time averaged value of Q.

ϵ	S
1.0	0.0849
1.5	0.2260
1.8	0.2937
2.0	0.3345
2.05	0.3444
2.1	0.3537
2.2	0.3721

TABLE 8. The variation of the parameter S as a function of ϵ.

The value of S has been calculated as function of ϵ and is shown in table 8. The value of $\frac{1}{2}\mu_1 \approx 0.3441$ from table 4. Thus the stability limit for the quasi-static case is attained when $\epsilon \approx 2.05$.

Appendix B. Definition of the Galerkin coefficients

In this Appendix we define the coefficients that appear in (54)–(57). Taking the dot product of (45) with Ψ_1'', we get

$$\nu_{11} = \langle Gr\,\Psi_1'', \Psi_1''\rangle, \quad \nu_{12} = \langle Gr\,\Psi_1^{*\prime\prime}, \Psi_1''\rangle, \tag{B 1a,b}$$

$$\nu_{13} = \langle ikGr[\psi_2(\Psi_2^{*\prime\prime\prime} - k^2\Psi_2^{*\prime}) - \psi_2^*(\Psi_2''' - k^2\Psi_2') + \psi_2'(\Psi_2^{*\prime\prime} - k^2\Psi_2^*) - \psi_2^{*\prime}(\Psi_2'' - k^2\Psi_2)], \Psi_1''\rangle, \tag{B 1c}$$

$$\nu_{14} = \langle \Psi_1^{\mathrm{iv}}, \Psi_1''\rangle, \quad \nu_{15} = \langle \Psi_1^{*\mathrm{iv}}, \Psi_1''\rangle, \quad \nu_{16} = \langle -\Theta_0', \Psi_1''\rangle, \tag{B 1d–f}$$

$$\nu_{17} = \langle -\Theta_1', \Psi_1''\rangle, \quad \nu_{18} = \langle -\Theta_1^{*\prime}, \Psi_1''\rangle. \tag{B 1g,h}$$

Similarly, taking the product of (46) with Θ_1, we get

$$\nu_{31} = \langle \Theta_1, \Theta_1\rangle, \quad \nu_{32} = \langle \Theta_1^*, \Theta_1\rangle, \quad \nu_{33} = \langle (\Psi_2\Theta_2^{*\prime} + \Psi_2'\Theta_2^*), \Theta_1\rangle, \tag{B 2a–c}$$

$$\nu_{34} = \langle (\Psi_2^*\Theta_2' + \Psi_2^{*\prime}\Theta_2), \Theta_1\rangle, \quad \nu_{35} = -\tau_B Ra\langle \Psi_1', \Theta_1\rangle, \tag{B 2d,e}$$

$$\nu_{36} = -\tau_B Ra\langle \Psi_1^{*\prime}, \Theta_1\rangle, \quad \nu_{37} = \langle \Theta_1'', \Theta_1\rangle, \quad \nu_{38} = \langle \Theta_1^{*\prime\prime}, \Theta_1\rangle. \tag{B 2f–h}$$

Taking the dot product of (47) with $\Psi_2'' - k^2\Psi_2$, we get

$$\nu_{21} = Gr\langle \Psi_2'' - k^2\Psi_2, \Psi_2'' - k^2\Psi_2\rangle, \tag{B 3a}$$

$$\nu_{22} = ikGr\langle [\Psi_2\Psi_0''' - (\Psi_2'' - k^2\Psi_2)\Psi_0'] - [\Psi_2^{\mathrm{iv}} - 2k^2\Psi_2'' + k^4\Psi_2], (\Psi_2'' - k^2\Psi_2)\rangle, \tag{B 3b}$$

$$\nu_{23} = ikGr\langle [\Psi_2\Psi_1''' - (\Psi_2'' - k^2\Psi_2)\Psi_1'], (\Psi_2'' - k^2\Psi_2)\rangle, \tag{B 3c}$$

$$\nu_{24} = ikGr\langle [\Psi_2\Psi_1^{*\prime\prime\prime} - (\Psi_2'' - k^2\Psi_2)\Psi_1^{*\prime}], (\Psi_2'' - k^2\Psi_2)\rangle, \tag{B 3d}$$

$$\nu_{21} = \langle \Theta_2', \Psi_2'' - k^2\Psi_2\rangle; \tag{B 3e}$$

and finally, taking the dot product of (48) with Θ_2 we obtain

$$\nu_{41} = Ra\langle \Theta_2, \Theta_2\rangle, \quad \nu_{42} = Ra\langle ik\Psi_2\Theta_0' - \tau_B\Psi_2', \Theta_2\rangle, \tag{B 4a,b}$$

$$\nu_{43} = ikRa\langle \Psi_2\Theta_1', \Theta_2\rangle, \quad \nu_{44} = ikRa\langle \Psi_2\Theta_1^{*\prime}, \Theta_2\rangle, \quad \nu_{45} = -ikRa\langle \Theta_2\Psi_1', \Theta_2\rangle, \tag{B 4c–e}$$

$$\nu_{46} = -ikRa\langle \Theta_2\Psi_1^{*\prime}, \Theta_2\rangle, \quad \nu_{47} = \langle -ikRa\,\Theta_2\Psi_0' - \Theta_2'' - k^2\Theta_2, \Theta_2\rangle. \tag{B 4f,g}$$

REFERENCES

ALEXANDER, J. I. D. 1990 Low gravity experiment sensitivity to residual acceleration: A review. *Microgravity Sci. Technol.* III **2**, 52–68.

ALEXANDER, J. I. D., AMIROUDINE, S., OUZZANI, J. & ROSENBERGER, F. 1991 Analysis of the low gravity tolerance of Bridgman–Stockbarger crystal growth II. Transient and periodic accelerations. *J. Cryst. Growth*, **113**, 21–38.

AMIN, N. 1988 The effect of g-jitter on heat transfer. *Proc. R. Soc. Lond.* A **419**, 151–172.

AUBRY, N., HOLMES, P., LUMLEY, J. L. & STONE, E. 1988 The dynamics of coherent structures in the wall region of a turbulent boundary layer. *J. Fluid Mech.* **192**, 115–173.

BATCHELOR, G. K. 1954 Heat transfer by free convection across a closed cavity between vertical boundaries at different temperatures. *Q. Appl. Maths* **12**, 209–233.

BERGHOLZ, R. F. 1978 Stability of natural convection in a vertical fluid layer. *J. Fluid Mech.* **84**, 743–768.

BIRINGEN, S. & DANABASOGLU, G. 1990 Computation of convective flow with gravity modulation in rectangular cavities. *J. Thermophys.* **4**, 357–365.

BIRINGEN, S. & PELTIER, L. J. 1990 Computational study of 3-D Benard convection with gravitational modulation. *Phys. Fluids* A **2**, 279–283.

BLOCH, F. 1928 Uber die Quantenmechanik der Elektronen in Kristallgittern. *Z. Phys.* **52**, 555–600.

DAVIS, S. H. 1976 The stability of time periodic flows. *Ann. Rev. Fluid Mech.* **8**, 57–74.

ELDER, J. W. 1965 Laminar free convection in a vertical slot. *J. Fluid Mech.* **23**, 77–98.

FAROOQ, A. & HOMSY, G. M. 1994 Streaming flows due to g-jitter-induced natural convection. *J. Fluid Mech.* **271**, 351–378.

GILL, A. E. 1966 The boundary layer regime for convection in a rectangular cavity. *J. Fluid Mech.* **26**, 515–536.

GRESHO, P. M. & SANI, R. L. 1970 The effects of gravity modulation on the stability of a heated fluid layer. *J. Fluid Mech.* **40**, 783–806.

HART, J. 1971 Stability of flow in a differentially heated inclined box. *J. Fluid Mech.* **47**, 547–576.

IYER, P. A. 1973 Instabilities in buoyancy driven boundary layer flows in a stably stratified medium. *Boundary-Layer Met.* **5**, 53–66.

KERCZEK, C. VON & DAVIS, S. H. 1974 Linear stability theory of oscillatory Stokes layers. *J. Fluid Mech.* **62**, 753–773.

KERCZEK, C. VON & DAVIS, S. H. 1976 Instability of a stratified periodic boundary layer. *J. Fluid Mech.* **75**, 287–303.

KLINE, S. J., REYNOLDS, W. C., SCHRAUB, F. A. & RUNSTADLER, P. W. 1967 The structure of turbulent boundary layers. *J. Fluid Mech.* **162**, 339–363.

MAGNUS, W. & WINKLER, S. 1966 *Hill's Equation.* Interscience.

MIZUSHIMA, J. & GOTOH, K. 1976 The stability of natural convection in a vertical fluid layer. *J. Fluid. Mech.* **73**, 65–75.

MOLER, C. B. & STEWART, G. W. 1973 An algorithm for generalized eigenvalue problems. *SIAM J. Numer. Anal.* **10**, 241–256.

NELSON, E. S. 1991 An examination of anticipated g-jitter on space station and its effects on materials processing. *NASA Tech. Mem.* 103775.

PAOLUCCI, S. & CHENOWETH, D. R. 1989 Transition to chaos in a differentially heated cavity. *J. Fluid Mech.* **201**, 379–410.

STOKER, J. 1950 *Non-linear Vibrations in Electrical and Mechanical Systems.* Wiley.

VEST, C. M. & ARPACI, V. S. 1969 Stability of natural convection in a vertical slot. *J. Fluid. Mech.* **36**, 1–15.